Yang *et al. Microstructures* 2024;4:2024042
DOI: 10.20517/microstructures.2024.06

Microstructures

Review

Open Access

Check for updates

TiO_2-based heterojunctions for photocatalytic hydrogen evolution reaction

Nan Yang[1], Tianwei He[1], Xinqi Chen[1], Yijun He[1], Tong Zhou[1], Genlin Zhang[1], Qingju Liu[1,2]

[1]National Center for International Research on Photoelectric and Energy Materials, Yunnan Key Laboratory for Micro/Nano Materials & Technology, School of Materials and Energy, Institute of International Rivers and Eco-Security, Yunnan University, Kunming 650091, Yunnan, China.
[2]Southwest United Graduate School, Kunming 650091, Yunnan, China.

Correspondence to: Dr./Prof. Tianwei He, National Center for International Research on Photoelectric and Energy Materials, Yunnan Key Laboratory for Micro/Nano Materials & Technology, School of Materials and Energy, Institute of International Rivers and Eco-Security, Yunnan University, Kunming 650091, Yunnan, China. E-mail: he.tianwei@ynu.edu.cn; Prof. Genlin Zhang, National Center for International Research on Photoelectric and Energy Materials, Yunnan Key Laboratory for Micro/Nano Materials & Technology, School of Materials and Energy, Institute of International Rivers and Eco-Security, Yunnan University, Kunming 650091, Yunnan, China. E-mail: 20070019@ynu.edu.cn; Prof. Qingju Liu, National Center for International Research on Photoelectric and Energy Materials, Yunnan Key Laboratory for Micro/Nano Materials & Technology, School of Materials and Energy, Institute of International Rivers and Eco-Security, Yunnan University, Kunming 650091, Yunnan, China; Southwest United Graduate School, Kunming 650091, Yunnan, China. E-mail: qjliu@ynu.edu.cn

How to cite this article: Yang N, He T, Chen X, He Y, Zhou T, Zhang G, Liu Q. TiO_2-based heterojunctions for photocatalytic hydrogen evolution reaction. *Microstructures* 2024;4:2024042. https://dx.doi.org/10.20517/microstructures.2024.06

Received: 20 Jan 2024 **First Decision:** 7 Mar 2024 **Revised:** 18 Mar 2024 **Accepted:** 1 Apr 2024 **Published:** 18 Jul 2024

Academic Editor: Quan Li **Copy Editor:** Fangling Lan **Production Editor:** Fangling Lan

Abstract

Solar-driven photocatalysis hydrogen evolution is a promising method to generate hydrogen from water, a green and clean energy source, using solar and semiconductors. Up to now, TiO_2 still represents the most inexpensive and widely studied metal oxide semiconductors for photocatalysis. TiO_2 coupling with other semiconductors to form heterojunctions is considered an efficient way to improve photocatalytic performances. In this review, TiO_2-based heterojunctions are classified into conventional, p-n type, Z-scheme, S-scheme, and other heterojunctions based on their band structures. The photocatalytic mechanisms of various types of heterojunctions are described in detail. In order to rationally design and better synthesize heterojunctions with excellent performance, the contribution of theoretical calculations to the field of TiO_2-based heterojunction photocatalysts and the key role of theoretical prediction are also discussed. Finally, the opportunities and current challenges to promote photocatalytic performance are provided to assist the design of TiO_2-based heterojunction photocatalysts with superior performance.

Keywords: TiO_2-based heterojunction, photocatalytic hydrogen evolution, DFT and experiment, heterojunction type

INTRODUCTION

Energy and environmental crises are the two key global issues in the wake of rapid industrial development and population growth[1-3]. Developing new and cleaner energy technologies to address the problems is extremely necessary[4,5]. Among the numerous emerging new energy technologies, photocatalysis hydrogen evolution technology that mainly utilizes solar energy to generate hydrogen from water is a clean, green, and environmentally friendly way and thus has been favored by increasing researchers[6-8].

Since the discovery by Fujishima in 1972, water could be decomposed into oxygen and hydrogen on TiO_2 electrodes under light[9]. TiO_2 represents a typical photocatalyst that is an inexpensive, environmentally friendly, and stable n-type semiconductor [Figure 1][10]. Currently, TiO_2-based photocatalysts play a pivotal role in the fields of pollutant degradation treatment, hydrogen evolution, and oxygen evolution [Figure 1]. Due to the high specific surface area of anatase TiO_2, more active electrons are generated more easily by photoexcitation. So, anatase TiO_2 is the most studied photocatalyst[11]. However, due to the wide bandgap of TiO_2, it is only responsive to ultraviolet (UV) light, limiting its development in photocatalysis[12,13]. To address this problem, it has been reported that coupling TiO_2 with other semiconductors to form heterojunctions can effectively improve the light absorption range and promote the separation of photogenerated electron-hole(e^-/h^+) pairs to enhance the photocatalytic activity. At present, researchers have developed a large number of TiO_2-based heterojunction photocatalysts, such as g-C_3N_4/TiO_2[14], b-N-TiO_2/Ag_3PO_4[15], and TiO_2/$FePS_3$[16].

In recent decades, TiO_2-heterojunction photocatalysts have achieved substantial advancements in photocatalytic H_2 evolution. This review primarily examines the progress of TiO_2 heterojunction modifications for H_2 evolution photocatalysis since 2019. Given the growing interest in photocatalytic H_2 evolution, summarizing recent studies on TiO_2-based heterojunction photocatalysts is crucial to propel practical applications. Herein, heterojunctions are categorized as Type-I, II, III, p-n, S-scheme, Z-scheme, and other semiconductor types based on energy band arrangement. Emphasis will be placed on (1) the mechanism of TiO_2 photocatalysis hydrogen evolution; (2) details of the mechanism of action of various types of heterojunctions and recent advances in the field of photocatalysis hydrogen evolution; (3) a summary and comparison of the hydrogen evolution rates for different types of heterojunction photocatalysts; (4) the importance of density-functional theory (DFT) calculation in the field of heterojunction photocatalysis is outlined; and (5) challenges and prospects for the construction of advanced TiO_2-based heterojunctions.

FUNDAMENTAL UNDERSTANDING OF PHOTOCATALYSIS HYDROGEN EVOLUTION

It is well known that the bandgap and position of band edges of a semiconductor are very important for photocatalysts. The bandgap needs to be at least 1.23 eV for water splitting. Moreover, the Conduction band (CB) edge should be more negative than the reduction potential of H_2 (E_{H_2O/H_2} = 0 V *vs.* NHE at pH = 0), and the Valence band (VB) edge should be more positive than the oxidation potential of O_2 (E_{O_2/H_2O} = 1.23 V *vs.* NHE at pH = 0)[17]. As shown in Figure 2, under light irradiation, when the energy of incident light ($h\nu$) is greater than or equal to the forbidden bandgap (E_g) of the semiconductor, the electron (e^-) in the VB will jump to the CB under photoexcitation, and at the same time, a hole (h^+) is left on the VB, after which the e^- and h^+ will migrate to the semiconductor surface. Then, the photogenerated electrons and holes will react with the adsorbates on the surface for reduction and oxidation reactions, respectively. At last, the products will be desorbed from the surface of the photocatalyst[18]. In photocatalytic hydrogen evolution, e^- will react

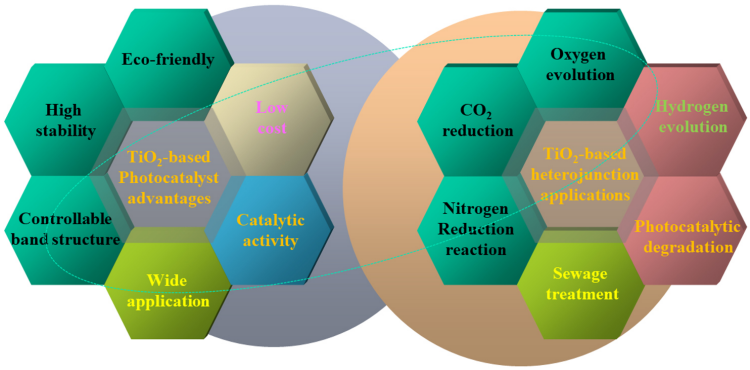

Figure 1. The advantages and applications of TiO_2-based photocatalysis heterojunctions.

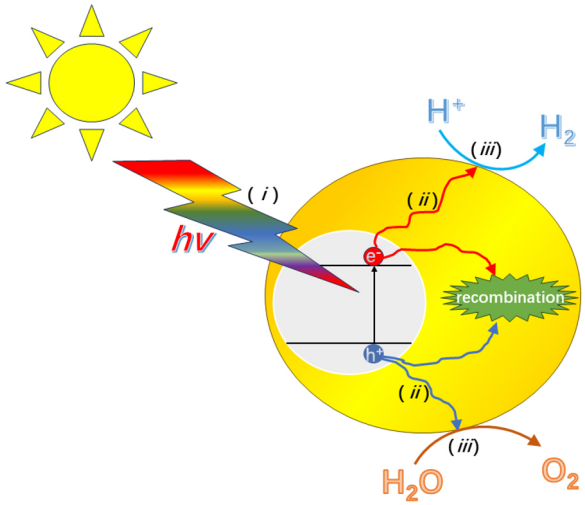

Figure 2. Schematic diagram of photocatalysis water splitting mechanism.

with H^+ in a reduction reaction to produce H_2, and h^+ will react with H_2O in an oxidation reaction to generate O_2[19]. However, some photogenerated e^-/h^+ pairs may combine during migration, which is unfavorable for photocatalysis[20]. In order to obtain high overall efficiency, rapid transfer of e^-/h^+ pairs to the surface while inhibiting the recombination of e^-/h^+ pairs is imperative but a huge challenge. TiO_2, due to the low efficiency of e^-/h^+ pairs separation and easier recombination, presents challenges for real application[21]. To improve the performances, researchers have put forward various methods. For example, Gao *et al.* introduced O vacancies based on N-doped TiO_2 and enhanced the photocatalysis hydrogen evolution rate to 3,183 $\mu molg^{-1}h^{-1}$[22]. An *et al.* reported Au clusters on a TiO_2 substrate, resulting in an astonishing two-order-of-magnitude increase in hydrogen evolution activity[23]. Although loading metal single atoms or clusters can improve the photocatalytic activity, the separation of photogenerated carriers remains limited. Whereas constructing heterojunctions has the advantages of heterojunctions in solving the photogenerated e^-/h^+ pairs combination, a detailed discussion of TiO_2-based heterojunctions in the field of photocatalysis hydrogen evolution will be given below.

TIO_2-BASED HETEROJUNCTION PHOTOCATALYSTS

The coupled heterojunctions could facilitate the separation of photogenerated carriers, reduce the recombination of e^-/h^+, and improve the photocatalysis efficiency. Heterojunctions can be classified into

traditional type-I, type-II, type-III, p-n heterojunction, Z-scheme, and emerging S-scheme heterojunction according to their energy band structures. Among them, the energy band structures of type I, type II, and type III are the straddling[24], staggered[25], and broken gaps[26], respectively. The p-n heterojunction composed of p- and n-type semiconductors with type-II energy band arrangement driven by built-in electric field[27], the Z-scheme heterojunction with electron-dielectric-driven charge separation[28], and the emerging S-scheme heterojunction formed by band bending due to the difference in Fermi energy levels[29].

Conventional semiconductor heterojunction photocatalyst

Conventional heterojunctions can be categorized into type-I, type-II, and type-III [Figure 3]. In straddling gap type-I heterojunction, the CB of semiconductor A and VB of semiconductor B are more negative than the CB of semiconductor B and VB of semiconductor A. In staggered gap type-II heterojunction, the CB and VB of semiconductor A are more negative than those of semiconductor B, respectively. In type-III heterojunction with a broken gap, both CB and VB of semiconductor A are more negative than CB of semiconductor B.

In type-I heterojunction, the electrons of both semiconductors transition from VB to CB and leave holes in the VB under the photoexcitation [Figure 3A]. Based on the characteristics of the band edge position, the h^+ will gather in the VB edge of semiconductor B, and photoelectrons will accumulate in the CB of semiconductor B. Among the three conventional heterojunctions, Type-II is one of the most popular photocatalysis heterojunctions studied due to its suitable energy band structure, band-edge position, and high photogenerated carrier separation efficiency. As shown in Figure 3B, when the two semiconductors are in contact, under light excitation, the e^- on the CB of semiconductor A will migrate to the CB of semiconductor B, and the holes on the VB of semiconductor B will gather on the VB of semiconductor A. The oxidation-reduction reaction will be conducted in the CB of semiconductor B and the VB of semiconductor A, respectively, so that the photogenerated e^-/h^+ pairs will be effectively separated, thus improving the photocatalysis activity[31]. Figure 3C demonstrates the structural features of type-III heterojunction photocatalysts. Obviously, in type-III heterojunction, both CB and VB of semiconductor B are more positive than those of semiconductor A. Such energy band relationship is not conducive to separating photogenerated electron-hole pairs[32], and the photocatalytic performance is inferior. Therefore, this review will not further elaborate on the TiO_2-based type-III heterojunction.

Table 1 summarizes the efforts and progress of TiO_2-based photocatalysis type-I and type-II heterojunctions for photocatalysis hydrogen evolution from 2019 to 2023. Cao *et al.* prepared Cu_2O/D-TiO_2 type-I heterojunctions, and a series of composites with Cu_2O contents ranging from 1% to 10% were synthesized[33]. Among them, the heterojunction with 5 wt% Cu_2O loading showed the highest H_2 evolution rate of 4.81 $mmol^{-1}h^{-1}$ under UV-visible light [Figure 4A-C]. The work functions of D-TiO_2 and Cu_2O were 4.69 and 5.46 eV, respectively. Only the e^- of the CB of D-TiO_2 flowed to the CB of Cu_2O when contacted in the dark environment. Under photoexcitation, both photogenerated e^-/h^+ pairs of D-TiO_2 transfer towards CB and VB of Cu_2O, respectively. Luo *et al.* prepared CdS quantum dots and ultrathin TiO_2(B) nanosheets by photodeposition and hydrothermal methods[34], respectively, where the heterojunction (PCT) prepared by photodeposition belongs to the type-II heterojunction and the heterojunction (HCT) prepared by hydrothermal method belongs to the type-I heterojunction [Figure 4D]. Under visible light excitation, 10-HCT will be excited only by CdS. However, under full-spectrum irradiation [Figure 4E], the photogenerated e^- and h^+ on the CB and VB of B-TiO_2 will be transferred to the CB and VB of CdS, respectively, which will improve the photocatalytic activity. Whereas in 5PCT [Figure 4F and G] and 5PCT(PVP) [Figure 4H and I], which satisfy the type-II energy band arrangement, the e^- on the CB of B-TiO_2 will be transferred to the CB of CdS under the visible-light excitation, while the holes are retained in the VB of B-TiO_2, and the full-spectrum irradiation will stimulate the hole transfer on the VB of CdS to the

Table 1. Comparison of typical type-I and type-II TiO_2-semiconductor heterojunctions in the last five years

Photocatalyst	Method	Light source	H_2-production rate ($\mu molg^{-1}h^{-1}$)	IPCE/photocurrent density	Year	Ref.
TiO_2/UiO-66-NH_2	Solvothermal	UV light	593.53	/	2022	[27]
Cu_2O/D-TiO_2	Solvothermal, photodeposition	Xe lamp	4,810	/	2023	[33]
CdS/$TiO_{2(B)}$	Hydrothermal	Xe lamp	1,776	/	2020	[34]
In_2S_3/TiO_2	Hydrothermal	Xe Arc lamp	/	2.82 $mAcm^{-2}$	2021	[35]
g-C_3N_4 quantum dots/a-TiO_2/r-TiO_2	Heat treatment	Simulated sunlight	49.3	/	2020	[36]
TiO_2 (A)/TiO_2 (R)/In_2O_3	One-step *in situ* calcination	Xe lamp	268	/	2022	[37]
TiO_2@$ZnIn_2S_4$ nanospheres	Hydrothermal	Xe lamp	4,958	/	2019	[38]
ZnO/$ZnCr_2O_4$@TiO_2-NTA	Electrochemical reduction-oxidation	Xe lamp	1,680	C	2019	[39]
Ti_3C_2@TiO_2/$ZnIn_2S_4$	Two-step hydrothermal	Xe lamp	1,185.8	/	2020	[40]
$BiVO_4$-TiO_2/rGO	Template	Xe lamp (420 nm)	6,998	20 $mAcm^{-2}$	2020	[41]
CdS/Ti^{3+}/N-TiO_2	Self-assembly, hydrothermal	Xe lamp (420 nm)	1,118.5	0.77 $mAcm^{-2}$	2020	[42]
GaAs (QD)/TiO_2	DFT	/	/	/	2021	[43]
3-$Cd_{0.5}Co_{0.5}S$/SN-TiO_2	Electrospinning	Xe lamp	4,550	/	2022	[44]
TiO_2 nanotubes/ZB CdS-CH_3COO-NPs	Electrospinning-solvothermal, chemical deposition	/	15,025.38	/	2022	[45]
TiO_2/$ZnIn_2S_4$/Co-Pt	Hydrothermal, annealing process	/	/	1.82 $mAcm^{-2}$	2022	[46]
3DOM CdS/In_2O_3-TiO_2 (Pt)	Colloidal crystal template	Xe lamp	3,428	/	2023	[47]
4.216TiO_2/CdS/g-C_3N_4	Hydrothermal, wet chemical, ultrasonic sonication processes	Xe lamp	116.5	4.16%/10.17 $mAcm^{-2}$	2023	[48]

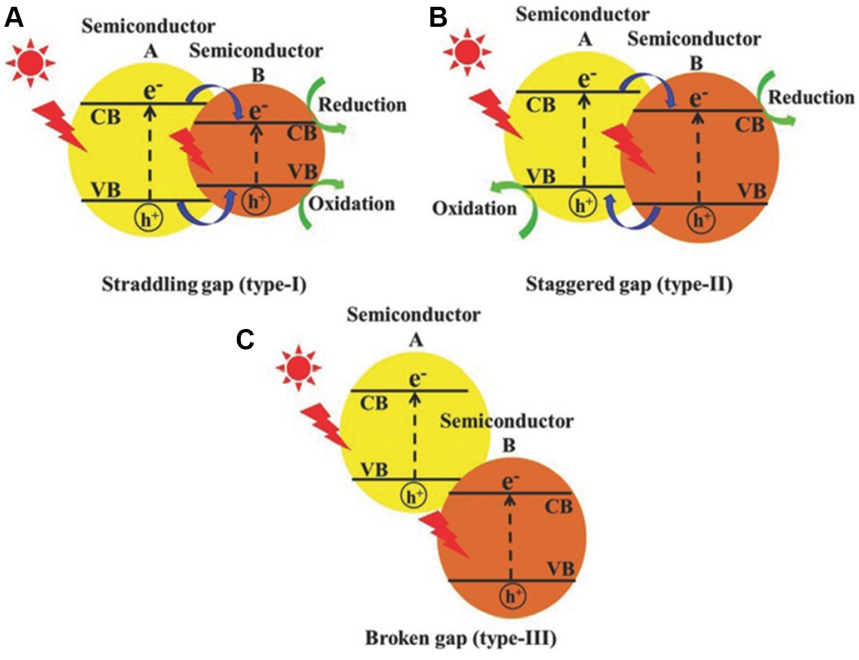

Figure 3. Schematic illustration of (A) type-I, (B) type-II, and (C) type-III heterojunctions. Quoted with permission from Low *et al.*[30].

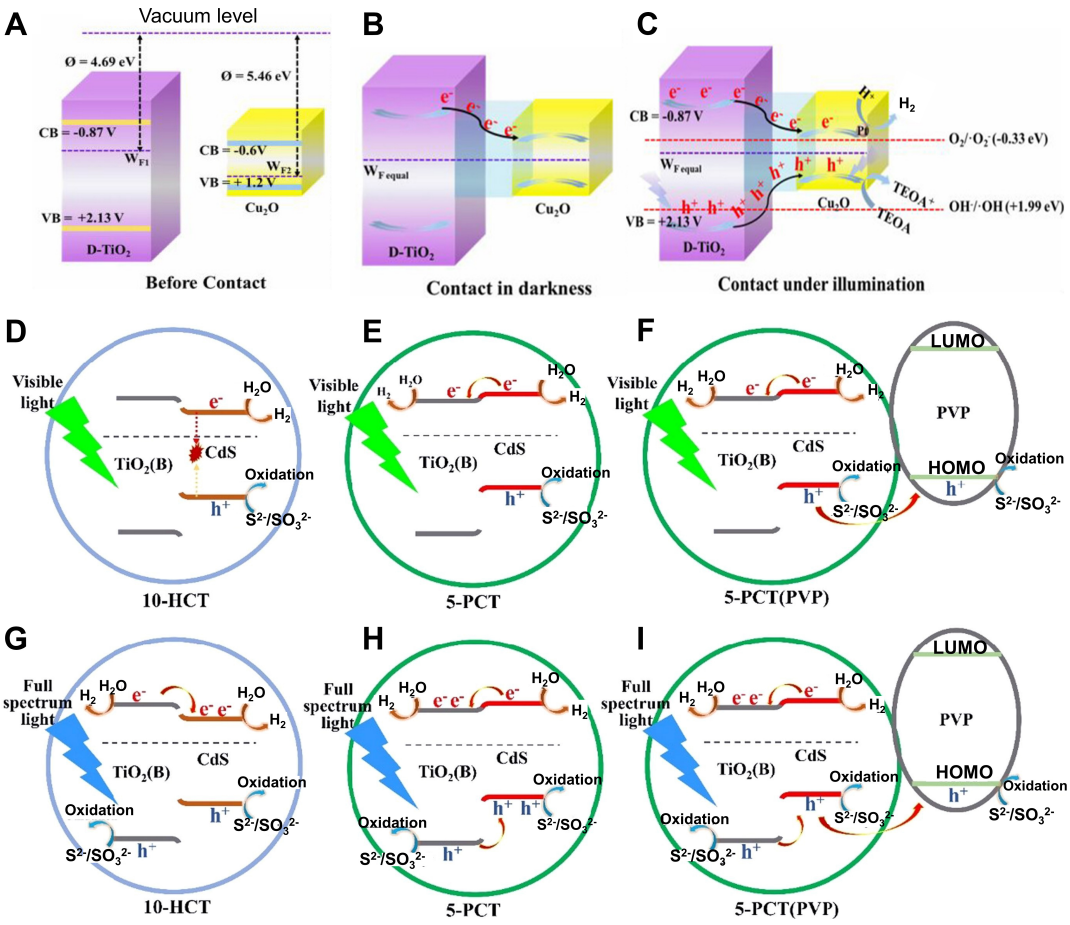

Figure 4. (A-C) Cu_2O/D-TiO_2 type-I heterojunction. Quoted with permission from Cao *et al.*[33]. (D-I) photocatalysis mechanism diagrams of 10-HCT, 5-PCT and 5-PCT (PVP). Quoted with permission from Luo *et al.*[34].

VB of B-TiO_2 at the same time based on the visible-light excitation, thus effectively separating the photogenerated carriers and improving the photocatalytic activity. The photocatalysis hydrogen evolution rates of 10-HCT and 5-PCT reach 11,317 and 34,937 $\mu molg^{-1}h^{-1}$, respectively. This shows that type-I heterojunction can improve the photocatalysis hydrogen evolution efficiency but is much less efficient than type-II heterojunction.

Type-I heterojunction effectively reduces the band gap and accelerates the photoexcited electron and hole transfer, However, it is rarely reported due to the difficulty of type-I heterojunction to separate the photogenerated e^-/h^+ pairs.

TiO_2/UiO-66-NH_2 type-II heterojunction was constructed by Kuang *et al.* by photo-induced activation treatment [Figure 5A and B][27]. Before contact, the CB and VB of UiO-66-NH_2 were more negative than those of TiO_2, respectively. After contact, under photoexcitation, *in situ* X-ray photoelectron spectroscopy (XPS) characterization revealed that UiO-66-NH_2 acted as an electron donor to transfer photogenerated electrons from the Lowest Unoccupied Molecular Orbital (LOMO) to CB of TiO_2, while h^+ of TiO_2 was transferred to the Highest Occupied Molecular Orbital (HOMO) of UiO-66-NH_2, which led to the separation of the photogenerated electron-hole pairs, the inhibition of the combination of photogenerated carriers, and the improvement of photocatalytic performance, with the photocatalytic hydrogen evolution

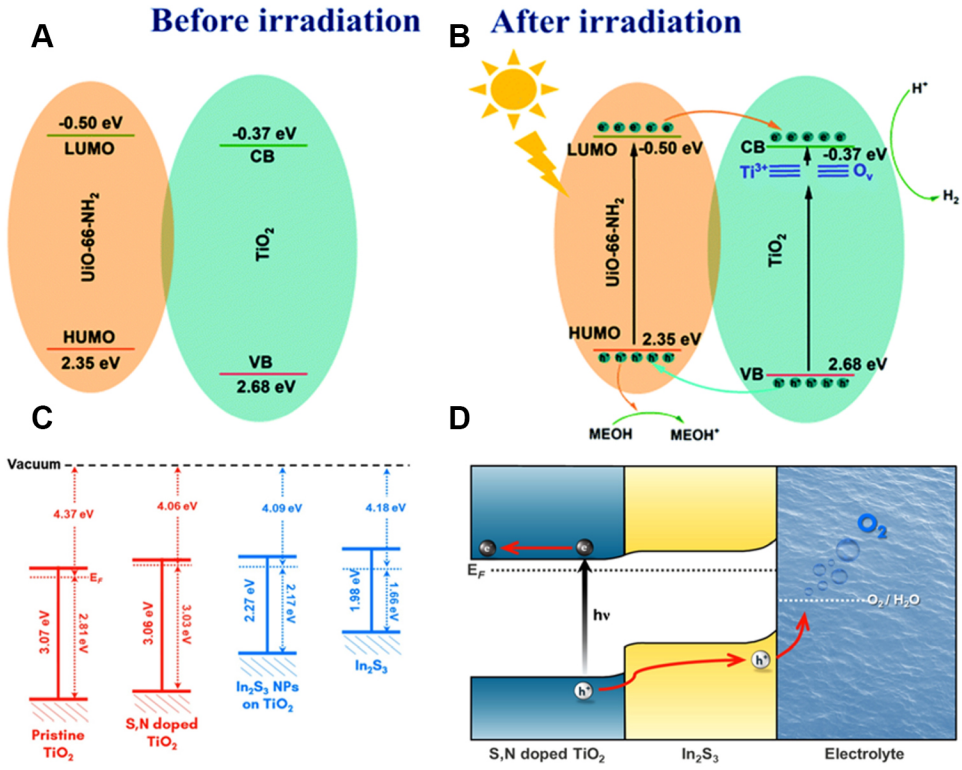

Figure 5. (A and B) Schematic diagram of UiO-66-NH_2 heterojunctions. (A and B) is quoted with permission from Kuang *et al.*[27]. (C) Energy band position of Pristine TiO_2, S, N-doped TiO_2, In_2S_3 NPs on TiO_2, and In_2S_3, (D) S, N-doped TiO_2/In_2S_3 heterostructure and photocatalytic mechanism diagrams. (C and D) is quoted with permission from Park *et al.*[35].

rate reaching 593.53 μmol$g^{-1}h^{-1}$. Park *et al.* synthesized In_2S_3/S, N-doped TiO_2 nanostructures by a hydrothermal method[35]; it has been observed that S, N doping significantly decreases the work function of TiO_2, enhances the electron concentration, effectively reduces the distance between CB and Ef, and increases the carrier concentration. Furthermore, the formation of In_2S_3/TiO_2 heterojunctions can effectively inhibit carrier combination, and its carrier lifetime is increased by a factor of 20 compared with that of the monomer. Specifically, the carrier lifetimes of TiO_2, S- and N-doped TiO_2, and S, N-doped TiO_2/In_2S_3 are 72.4, 50.3 ns, and 1.16 μs. The band edge positions [Figure 5C] show that the VB and CB of the S, N-doped TiO_2 are more positive than those of In_2S_3. This conforms to the type-II energy band arrangement, and the bandgap of the heterojunction is only 2.27 eV. Under the photoexcitation [Figure 5D], h^+ will accumulate on the VB of In_2S_3, while e^- will gather on the CB of S, N-doped TiO_2. Ultimately, the oxygen evolution (OER) and hydrogen evolution reactions will be performed on the VB of In_2S_3 and the CB of S, N-doped TiO_2, respectively, thus realizing photocatalytic water splitting.

In addition, the excellent photocatalysis properties of binary type-II heterojunctions have led to great interest in ternary and even multicomponent type-II heterojunctions. Recently, Zhou *et al.* have designed a Type-II/Type-II energy band arrangement of g-C_3N_4 quantum dots/a-TiO_2/r-TiO_2 heterojunctions for photocatalysis total water splitting[36]. Figure 6A-F shows the Type-II/Type-I and Type-II/Type-II energy band arrangement and photocatalytic mechanism diagrams. In addition, its photocatalysis hydrogen and oxygen evolution efficiencies reached 1,526.4 and 198.8 μmol h^{-1}, respectively, and it can be extended to the decomposition of methylene blue (MB). Yang *et al.* prepared Mxene-derived anatase-TiO_2/rutile-TiO_2/In_2O_3 heterojunctions to enhance the hydrogen evolution rate to 1,488 times that of In_2O_3[37].

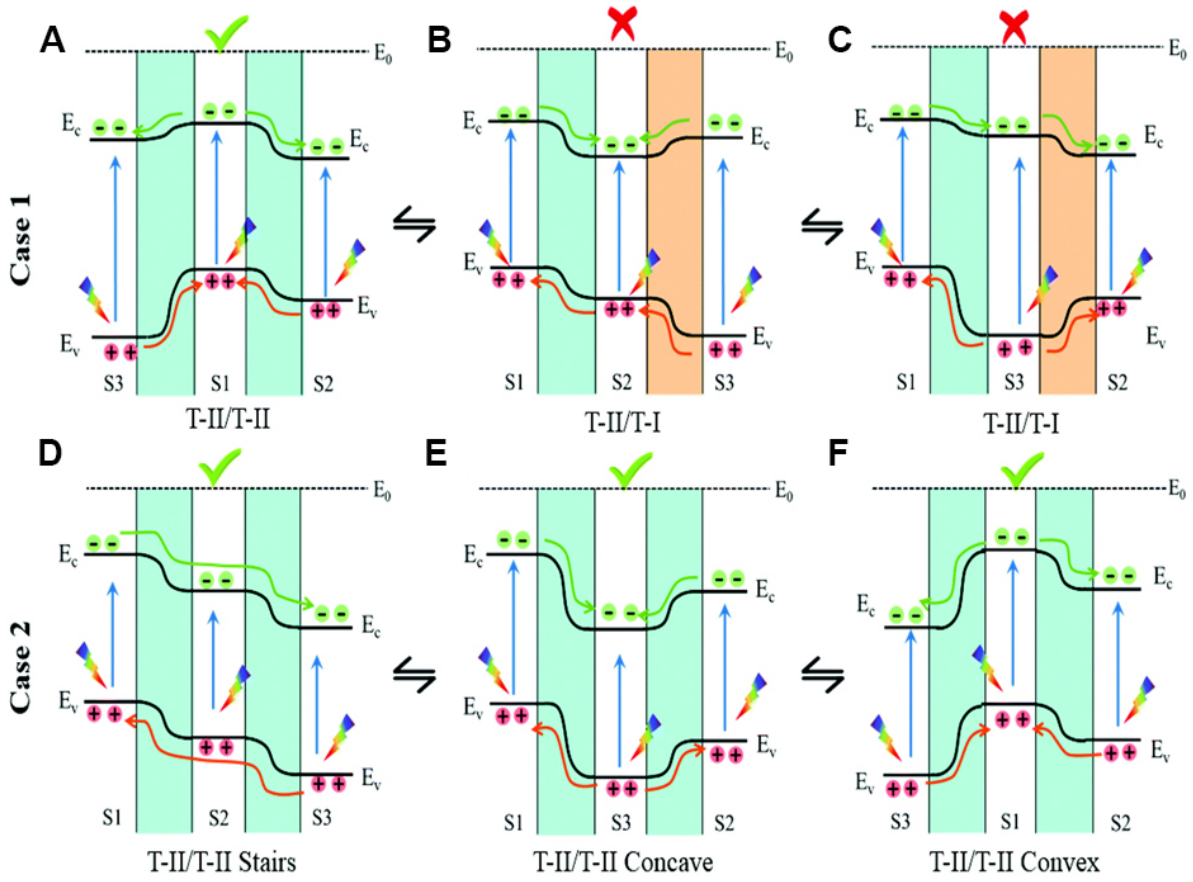

Figure 6. (A-F) Energy band arrangements and photocatalytic mechanisms diagrams of T-II/T-II, T-II/T-I, T-II/T-II Stairs, T-II/T-II Concave and T-II/T-II convex. Quoted with permission from Zhou *et al.*[36].

Although type II heterojunctions can effectively inhibit the compounding of photogenerated electron-hole pairs, their study is limited by the fact that the original electrons inside the semiconductor will impede the foreign electron transport, which results in a significant reduction of their oxidation-reduction capability.

p-n heterojunction photocatalysts

The reaction mechanism of p-n heterojunction photocatalysis differs from that of type-II heterojunctions. In p-n heterojunctions, photocatalytic efficiency enhancement primarily stems from energy band engineering and improved carrier separation driven by internal electric fields (IEF)[31]. As illustrated in Figure 7A and B, p-n heterojunctions have two different type-II energy band arrangements[31]. Both generate an IEF pointing from the n- to the p-type semiconductor in the heterojunction formation[49]. In Figure 7A, the CB and VB of p-type semiconductors in the first type of p-n heterojunction are higher than those of n-type semiconductors, respectively, and e^- will be transferred from the CB of the p-type semiconductors to the CB of the n-type semiconductors and h^+ will be transferred from the VB of the n-type semiconductors to the VB of the p-type semiconductors[50]. Since the direction of the IEF is the same as that of charge transfer, the separation of e^-/h^+ pairs is accelerated by the IEF. However, in the second type of p-n heterojunction [Figure 7B], the type-II energy band arrangement is opposite to that of Figure 7A, and the e^- will be transferred from CB of an n-type semiconductor to CB of a p-type semiconductor, and the h^+ will be transferred from VB of a p-type semiconductor to VB of an n-type semiconductor. In this case, we will find that the direction of IEF is opposite to that of the charge transfer, which will result in the separation

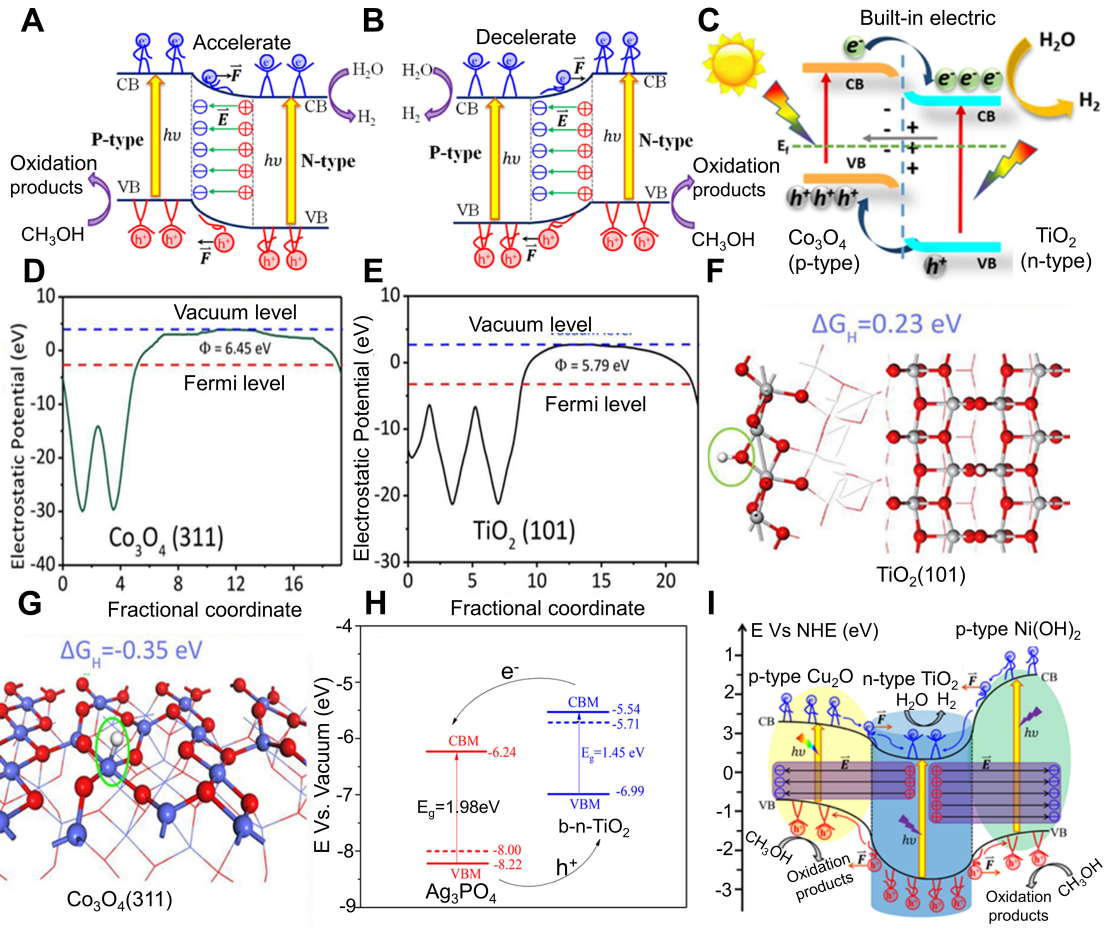

Figure 7. Type-II energy band arrangement of (A) the first type and (B) the second type of p-n heterojunction. (A, B, I) is quoted with permission from Ding *et al.*[49]. (C) catalysis mechanism of Co_3O_4/TiO_2. (D and E) G_H of TiO_2 and Co_3O_4 and (F and G) work function for the TiO_2 and Co_3O_4 facets. (C-G) is quoted with permission from Wang *et al.*[54]. (H) band structure diagram for Ag_3PO_4/b-N-TiO_2. (H) is quoted with permission from Zhou *et al.*[15]. (I) The charge segregation mechanism of $Cu_2O/Ni(OH)_2/TiO_2$.

decelerated by restricting the movement of the e^-/h^+ pairs[31]. In addition to the above two types of p-n heterojunctions, some researchers have also suggested that the mechanism of the second type of p-n heterojunctions should be consistent with the direct Z-scheme heterojunctions[51-53]. The distinction and categorization of p-n and direct Z-scheme heterojunctions has been controversial. Therefore, their difference should be thoroughly verified in future heterojunction studies.

The above two p-n heterojunctions with different action mechanisms have been reported and synthesized experimentally in many cases [Figure 7C-G]. Wang *et al.* synthesized 2D/1D and 3D/1D Co_3O_4/TiO_2 composites by a hydrothermal method with a hydrogen evolution rate of up to 3,460 $\mu molg^{-1}h^{-1}$[54], and DFT calculations were used to explore the reason for their high activity. Theoretical calculations show that the Fermi level of Co_3O_4 is significantly higher than that of TiO_2 [Figure 7D and E], resulting in a greater e^- transfer to TiO_2 and a significant increase in electron concentration. Additionally, due to the difference in Fermi energy levels, an IEF is generated within TiO_2 towards Co_3O_4, accelerating the transfer of e^- from the CB of Co_3O_4 to that of TiO_2 and h^+ from the VB of TiO_2 to that of Co_3O_4. This effectively promotes photogenerated carrier separation, increases carrier concentration, and improves catalytic activity. Figure 7F and G shows the Gibbs free energies after heterojunction formation on TiO_2 and Co_3O_4 of 0.23 and -0.35 eV, respectively. As reported in Figure 7H, Zhou *et al.* reported p-n heterojunctions have opposite

band edge positions[15]; the CB of Ag_3PO_4 is lower than the CB of b-N-TiO_2, and the VB of Ag_3PO_4 is higher than the VB of b-N-TiO_2. An IEF pointing from b-N-TiO_2 to Ag_3PO_4 will be generated at the interface, which balances the Fermi energy levels, leading to a photogenerated e^-/h^+ pairs separation by moving the e^- at the CB of b-N-TiO_2 towards the CB of Ag_3PO_4, while the h^+ move in the opposite direction of the e^-. Overall, the p-n heterojunctions composed of two different type-II energy band arrangements both can effectively improve the transfer and separation of electron-hole pairs and the photocatalytic activity.

Table 2 summarizes some of the applications of p-n type heterojunctions for photocatalytic hydrogen evolution from 2019 to 2023. Most current research has focused on synthesizing a single p-n heterojunction, which is certainly effective, but the utilization efficiency of photogenerated e^-/h^+ pairs is still poor. Accordingly, researchers have begun to turn their attention to exploring dual p-n type heterojunctions. As presented in Figure 7I, Ding *et al.* adopt chemical precipitation and ultrasound-assisted glucose reduction to synthesize $Ni(OH)_2/TiO_2$,Cu_2O/TiO_2 and $Cu_2O/Ni(OH)_2/TiO_2$ photocatalysts[49]. It is found that the hydrogen evolution rate of $Cu_2O/Ni(OH)_2/TiO_2$ is 6,145 $\mu molg^{-1}h^{-1}$ which is much higher than that of $Ni(OH)_2/TiO_2$ (3,265 $\mu molg^{-1}h^{-1}$) and Cu_2O/TiO_2 (2,285 $\mu molg^{-1}h^{-1}$). The excellent photocatalytic activity is attributed to the synthesized $Cu_2O/Ni(OH)_2/TiO_2$ being a fully depleted p-n junction with IEF. Under photoexcitation, the e^- on the CB of $Ni(OH)_2$ and Cu_2O will be transferred to the CB of TiO_2 because the CB of TiO_2 is more positive than the CB of $Ni(OH)_2$ and Cu_2O, while the h^+ will be transferred from the VB of TiO_2 to the VB of $Ni(OH)_2$ and Cu_2O, respectively, because the VB of TiO_2 is more positive. The direction of the IEF is directed from TiO_2 to $Ni(OH)_2$ and Cu_2O, respectively, which is opposite to the motion direction of the e^- and the same as that of the h^+, thus promoting the carrier migration and effectively improving the separation of the photogenerated e^-/h^+ pairs, which effectively improves the photocatalytic activity. In addition, Chen *et al.* prepared a 3D g-C_3N_4-Cu_2O-TiO_2 by a sacrificial template strategy and photo-deposition with a maximum hydrogen evolution rate of 12,108 $\mu mol\ g^{-1}h^{-1}$[55]. Overall, p-n heterojunction plays an indispensable role in heterojunction catalysts due to their unique energy band properties and excellent photocatalytic activity, but it does not overcome the disadvantages of the type II heterojunction.

Z-scheme heterojunction photocatalysts

Comparing the limited carrier oxidation-reduction capacity of type-II and p-n heterojunctions, the Z-scheme can not only effectively promote carrier separation but also enhance the carrier oxidation-reduction capacity. Z-scheme heterojunctions can be classified into three main categories: liquid-phase, all-solid-state, direct, and dual.

The liquid-phase Z-scheme heterojunction [Figure 8A] is characterized by a pair of electron acceptor-donor (A-D) between the two semiconductors as a transport medium for e^-[65]. At this time, the e- on CB of semiconductor 1 and the h^+ on VB of semiconductor 2 will react within A and D, respectively. After the formation of the heterojunction, the oxidation reaction is carried out on the VB of semiconductor 1, and the reduction reaction is conducted on the CB of semiconductor 2, which effectively separates the photogenerated carriers. However, the existence of the reverse reaction and the light shielding effect will reduce the number of e^- and h^+. In addition, the liquid medium is easy to deactivate, and all of these uncertainties will affect the photocatalytic activity to a certain extent[17].

The all-solid-state Z-scheme heterojunction is proposed to circumvent the disadvantages of liquid-phase Z-scheme heterojunction. Its main feature is to insert a piece of conductor between two semiconductors to promote carrier migration and improve photocatalytic activity. For example [Figure 8B], Han *et al.* reported that Au was inserted as the most electron-mediated medium between TiO_2 and TrTh[66]. At this time, the e^- of CB of TiO_2 would combine with the h^+ on the VB of TrTh through Au, and the oxidation and reduction

Table 2. Comparison of selected research results on TiO_2-based p-n heterojunction photocatalytic hydrogen evolution from 2019 to 2023

Photocatalyst	Method	Light source	H_2-production rate ($\mu molg^{-1}h^{-1}$)	IPCE/photocurrent density	Year	Ref.
$Cu_2O/Ni(OH)_2/TiO_2$	Hydrothermal, calcination	Xe lamp	6,145	/	2021	[49]
CuS/TiO_2	Solvothermal	Xe lamp	705.8	/	2023	[50]
0D Co_3O_4/1D TiO_2	Hydrothermal, electrospinning	Xe lamp (200-780 nm)	3,460	/	2022	[54]
g-C_3N_4-Cu_2O-TiO_2	Sacrificial template, photodeposition	/	12,108	/	2021	[55]
Cu_2O/TiO_2 (P25)	One-pot hydrothermal	Xe lamp ($\lambda > 420$ nm)	2,550	0.75 $mAcm^{-2}$	2021	[56]
NiO-TiO_2	Sol-gel, hydrothermal	Xe lamp	23,500	/	2021	[57]
$Co_{0.85}Se/TiO_2$	Two-step hydrothermal	Xe lamp (365 nm)	2,312.5	10 $mAcm^{-2}$	2022	[58]
$Cu_3Mo_2O_9/TiO_2$	Mechanical mixing	Xe lamp (350-780 nm)	3,401.9	6.4 $mAcm^{-2}$	2022	[59]
Co_3O_4/Ti^{3+}-TiO_2/NiO	Chemical-hydrothermal-annealing-reduction	/	2,134.63	/	2022	[60]
Cu_2NiSnS_4/TiO_2(B)	Hydrothermal	Direct sunlight	7,144	/	2023	[61]
Li@g-C_3N_4/F@TiO_2-B(001)	DFT	/	/	/	2023	[62]
$Ni(OH)_2$-TiO_2-Cu_2O	Hydrothermal-calcination	Xe lamp	8,384.84	/	2023	[63]
NiO-TiO_2	Hydrothermal	Xe lamp	8,000	/	2023	[64]

reactions would take place on the VB of TiO_2 and the CB of TrTh, respectively. The selection and design of electron mediators is a particularly important aspect in all-solid-state Z-scheme heterojunctions. However, the high price of the electronic medium seriously limits the development of the all-solid-state Z-scheme heterojunction.

In 2009, Wang *et al.* addressed the challenge of costly all-solid-state Z-scheme heterojunctions by introducing electron-mediator-free, direct-contact Z-schemes[67]. In 2013, Yu *et al.* further proposed direct Z-scheme heterojunctions enhanced by IEF[68]. The key distinction of this design from liquid Z-schemes lies in its elimination of the need for an electron transfer medium. As illustrated in Figure 8C, when TiO_2 and $ZnIn_2S_4$ form a heterojunction, their energy bands align in a staggered configuration due to disparities in Fermi energy levels and work functions, causing band bending at the contact interface. IEF direct from $ZnIn_2S_4$ towards TiO_2, and coupled with band bending, facilitates electron transfer from the CB of TiO_2 to the VB of $ZnIn_2S_4$ to recombine with h^+, while simultaneously impeding the reverse flow of electrons from the CB of $ZnIn_2S_4$ and holes from the VB of TiO_2. This mechanism both guarantees sufficient charge carriers for redox reactions and spatially separates photogenerated carriers, thereby contributing to enhanced photocatalytic performance.

The direct Z-scheme has been widely studied in academia due to its unique energy band structure and efficient photocatalytic ability. Consequently, we will focus on the direct Z-scheme heterojunctions in photocatalysis hydrogen evolution. Ran *et al.* used liquid exfoliation, precipitation-hydrothermal methods to prepare the $ReSe_2/TiO_2$ direct Z-scheme heterojunctions[69]. These prepared heterojunctions exhibited a photocatalysis hydrogen evolution rate of up to 2,081 $\mu molg^{-1}h^{-1}$ and were combined with DFT to show that the presence of an IEF promotes the electron transfer from TiO_2 to $ReSe_2$. Moon *et al.* successfully synthesized the Pt/g-$C_3N_4/TiO_2/IrO_x$ heterojunctions [Figure 8D] through the classical Stöber method[70]. The formation of Z-scheme heterojunctions [Figure 8E] accelerated the surface charge separation and

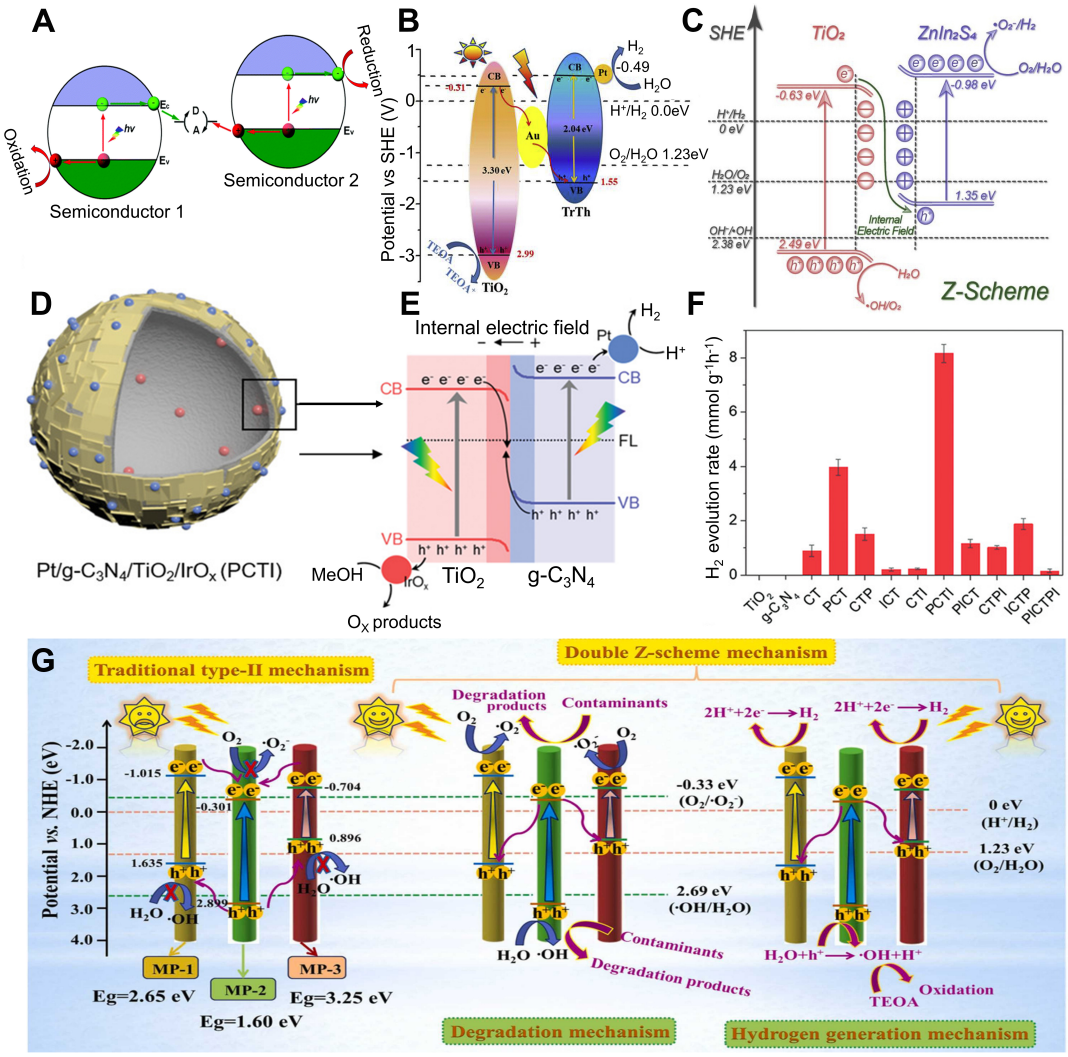

Figure 8. (A) liquid-phase Z-scheme heterojunction. Quoted with permission from Bai *et al.*[65]. (B) Au@TiO_2-12%TrTh all-solid-state Z-scheme heterojunction. Quoted with permission from Han *et al.*[66]. (C) photocatalytic mechanism of TiO_2-$ZnIn_2S_4$ nanoflowers. Quoted with permission from Zuo *et al.*[71]. (D) physical structure of Pt/g-C_3N_4/TiO_2/IrO_x (PCTI). (E) The charge-transfer process within PCTI upon light irradiation. (F) H_2 evolution rate. (D-F) is quoted with permission from Moon *et al.*[70]. (G) Photocatalytic mechanism diagram of double Z heterojunction TMOP. Quoted with permission from Sun *et al.*[72].

reaction kinetics, resulting in catalysts with apparent quantum yields, hydrogen evolution rates, and oxygen evolution rates as high as 24.3%, 8.15 $mmolg^{-1}h^{-1}$ [Figure 8F], and 443.9 $\mu molg^{-1}h^{-1}$, respectively. Photogenerated e^- was reduced to H_2 on the CB of Pt/g-C_3N_4 and h^+ was oxidized to oxygen on the VB of TiO_2/IrO_x to achieve total water splitting.

Double Z-scheme heterojunction can further enhance the separation of photogenerated e^-/h^+ pairs and improve the photocatalytic activity. As shown in Figure 8G, MP-1, MP-2, and MP-3 are contacted to form a double Z-scheme heterojunction. After photoexcitation, the e^- on the CB of MP-2 will combine with the h^+ on the VB of MP-1 and MP-3, respectively. The remaining photogenerated e^- on the CB of MP-1 and MP-3 will participate in the reduction reaction, and the h^+ on the VB of MP-2 will engage in the oxidation reaction. It should also be noted that the double Z-scheme heterojunction is not a simple superposition of the three components but rather utilizes the synergistic effect among them to accelerate the electron transfer

and the separation of the photogenerated carriers to extend the lifetime of the carriers, thus improving the photocatalytic activity.

Table 3 demonstrates some research results of TiO_2-based Z-scheme heterojunctions in photocatalysis hydrogen evolution from 2019 to 2023.

S-scheme heterojunction photocatalysts

Xu *et al.* reported the first S-scheme heterojunction photocatalysts in 2019[29]. Zhang *et al.* extended the S-scheme heterojunction which can only be of an n-n type to n-p, p-n, p-p type in 2022[86]. However, the condition is that the CB position and Fermi energy level of the reduced semiconductor (RP) should be higher than those of the oxidized semiconductor (OP) simultaneously at this time; the OP and RP can be either n- or p-type semiconductors [Figure 9A-D]. As in Figure 9E-G, taking the n-n junction as an example, when both the CB and E_f of RP are higher than those of OP, due to the difference in E_f, an IEF pointing from RP to OP will be formed between the interfaces, which will lead to the energy band bending, and the photogenerated e^- on the CB of OP and the photogenerated h^+ on the VB toward RP will be combined under the action of the IEF. The h^+ on the VB of OP and the e^- on the CB of RP will stay on the energy band due to the bending of the energy band, which promotes the separation of the photogenerated e^-/h^+ pairs. In the photocatalytic process, oxidation-reduction reactions will be carried out by the e^- and h^+ retained in RP and OP, respectively[87]. Overall, S-scheme heterojunctions greatly enhance photocatalytic efficiency due to their strong oxidation-reduction capacity and unique carrier migration mode. However, currently, S-scheme heterojunctions are mostly focused on powder catalysts, and their kinetics need to be well studied and understood. Finally, Table 4 summarizes the 2020 to 2024 S-scheme TiO_2-based heterojunctions for photocatalytic hydrogen evolution.

Other TiO_2-based photocatalytic heterojunctions

In addition to the common type-II, p-n, Z-scheme, and S-scheme heterojunctions discussed above, researchers have also devoted themselves to studying 2D van der Waals heterojunction formed by the IEF dominated by van der Waals forces, phase heterojunction formed by the same semiconductor that exists only in several different crystalline phases, facet heterojunction dominated by exposed surfaces, and Schottky heterojunction formed by semiconductor interacting with metal[104]. However, these heterojunctions are mostly used for the degradation of organic matter and the photoreduction of CO_2, and fewer of them have been applied to the photocatalytic hydrogen evolution [Table 5], so they will not be specifically discussed in this review.

Application of DFT calculation to investigate TiO_2-based photocatalytic heterojunctions

In recent years, theoretical calculations based on DFT can provide accurate predictions of the electronic structure, optical properties, and photocatalytic activity of materials[19]. The first is the binding energy of the heterojunction. In DFT calculations, the positive and negative values of the binding energy of the heterojunction can determine whether the two semiconductors need external energy injection in the coupling process. Next, the value of the binding energy can qualitatively determine the difficulty of forming heterojunctions for different semiconductors. Secondly, DFT calculations can confirm the amount of electron transfer in the heterojunction and the direction of charge transfer. Wang *et al.* constructed 0D/2D Co_3O_4/TiO_2 Z-scheme heterojunctions, and DFT calculations demonstrated that the work functions of Co_3O_4 and TiO_2 were 5.69 and 4.84 eV, respectively[51]. The difference in the Fermi energy levels drove the charge transfer from TiO_2 to Co_3O_4. Moreover, the hybrid function calculations can accurately obtain the bandgap, HOMO, and LOMO of semiconductors. Density of states (DOS) can analyze the coupling of impurity orbitals in the forbidden bands of semiconductors after modification in a more detailed way and explore the essential reasons for the catalytic performance enhancement of semiconductor catalysts more

Table 3. Some research results of Z-scheme TiO_2-based heterojunction for photocatalytic hydrogen evolution from 2019 to 2023

Photocatalyst	Method	Light source	H_2 production rate ($\mu molg^{-1}h^{-1}$)	IPCE/photocurrent density	Year	Ref.
Au@TiO_2-X%TrTh	Situ polymerization	Visible light	4,288.54	0.13 μAcm^{-2}	2022	[66]
$ReSe_2/TiO_2$	Liquid exfoliation, hydrothermal, DFT	Xe lamp	2,081	/	2023	[69]
Pt/g-$C_3N_4/TiO_2/IrO_x$	Classical Stöber	Xe lamp	8,150	/	2022	[70]
TiO_2-$ZnIn_2S_4$	Hydrothermal, DFT	Xe lamp	18,077.2	/	2021	[71]
TMOP Tricolor-typed microfiber	Tri-axial parallel electrospinning technology	Simulated sunlight	536.7	/	2023	[72]
3D/2D TiO_2 /g-C_3N_4	Hydrothermal	Xe lamp	4,128	/	2019	[73]
fluorinated-TiO_2 /CdSe-DETA	Mild solvothermal	Xe lamp ($\lambda \geq 420$ nm)	12,381	/	2020	[74]
ZrO_2@TiO_2	Solvothermal, calcinating	Xe lamp	39,700	/	2020	[75]
$Bi_2S_3/MoS_2/TiO_2$	Facile microwave-assisted hydrothermal	Xe lamp ($\lambda \geq 420$ nm)	2,195	/	2020	[76]
Ni $(OH)_2$-Cu_xO-TiO_2	Hydrothermal	tungsten halogen lamp	15,789	/	2020	[77]
g-C_3N_4/TiO_2@Pt	Hydrothermal	Xe lamp	15,360	15 μAcm^{-2}	2021	[78]
Cu_2O/TiO_2	Hydrothermal, DFT	Xe lamp	14,020	20 μAcm^{-2}	2021	[79]
MoS_2 /TiO_2 nanosheets	Spin coating	Xe lamp (420 nm)	5,423.77	/	2022	[80]
2D/2D TiO_2/g-C_3N_4	Thermal polymerization, colloidal, electrostatic self-assembly	Xe lamp (380 nm)	3,875	/	2022	[81]
$ZnIn_2S_4/TiO_2$(MOFs)	Hydrothermal, calcination	Xe lamp (400 nm)	2,451.5	1.42 μAcm^{-2}	2023	[82]
Bi_2WO_6/TiO_2	One-step solvothermal	Xe lamp	12,900	/	2023	[83]
g-C_3N_4/TiO_2 nanotube	Electrospinning	/	4,122	/	2023	[84]
TiO_2 (116)/red phosphorus (001)	Chemical vapor deposition	/	12.9($\mu mol \cdot h^{-1}$) ($\lambda > 300$ nm)	/	2023	[85]

precisely. For example, Li *et al.* constructed defective RuO_2/TiO_2 heterostructures [Figure 10A-C][107]. DFT calculations showed that Ru defects were surrounded by more positrons, which favors water decomposition, and the Gibbs free energy after the formation of the heterojunction decreased from 0.32 to -0.12 eV, which accelerates the separation of photogenerated e^-/h^+ pairs by the interfacial effect of the heterostructures, decreases the adsorption energy of H_2, and accelerates the precipitation of hydrogen. Di Liberto *et al.*[108]. proposed the $SrTiO_3/TiO_2$ [Figure 10D-E] heterostructure and found that the CB and VB of $SrTiO_3$ became more positive after the heterojunction formation and conformed to the type-II energy band arrangement with TiO_2 by hybrid functional theory calculations. Li *et al.* put forward a TiO_2/ZnS heterojunction and investigated the electronic properties and excitation electron dynamics heterostructure by using Vienna ab-initio simulation package (VASP) and NAnoscale Molecular Dynamics (NAMD)[99]. It was found that [Figure 10F-H] the work functions of TiO_2, ZnS, and TiO_2/ZnS were 6.89, 5.74, and 5.80 eV, respectively. The differences in the work functions and the Fermi energy levels resulted in the transfer of e- from ZnS to TiO_2 until the charge equilibrium at the interfaces. The plane-averaged and differential charge densities demonstrated in Figure 10I proved the existence of strong interactions between the interfaces. In addition, [Figure 10J-K] the light absorption is significantly enhanced, and the STH conversion efficiency is as high as 23.46% both in acidic, neutral, and alkaline environments. Although DFT calculations have matured and provided much effective guidance for experiments, providing effective support for catalytic mechanisms, they still have many limitations. First, the bandgap of semiconductors is often underestimated in Perdew-Burke-Ernzerhof (PBE) calculations. While DFT + U, DFT-1/2 and Hybrid functional methods have been proposed to correct the bandgap value, they encounter multiple constraints, such as the lack of

Table 4. Comparison of some research results of S-scheme TiO_2-based heterojunction photocatalysis hydrogen evolution from 2020 to 2024

Photocatalyst	Method	Light source	H_2-production rate ($\mu molg^{-1}h^{-1}$)	IPCE/photocurrent density	Year	Ref.
α-Fe_2O_3/TiO_2-Pd	Impregnation	UV lamp ($\lambda \geq 420$ nm)	3,490.54	/	2021	[88]
3D/2D/0D TiO_2/g-C_3N_4/Ti_3C_2 QDs	Solvothermal reaction, DFT	Xe lamp (420 nm)	5,540.21	/	2021	[89]
Co_2P/PC-b-TiO_2	Pyrolyzing a mixture of cobalt phosphonate and TiO_2 under H_2 atmosphere	Xe lamp	1,530	/	2022	[90]
$ZnCo_2S_4/TiO_2$	Solvothermal	Xe lamp (420 nm)	5,580	/	2022	[91]
Co_3Se_4/TiO_2	Hydrothermal	Xe lamp (350-780 nm)	6,065	/	2022	[92]
1D/2D $TiO_2/ZnIn_2S_4$	Hydrothermal	LED lamp (365 nm)	6,030	/	2022	[93]
O-$ZnIn_2S_4/TiO_{2-x}$	Hydrothermal, liquid assembly, DFT	Xe lamp (420 nm)	2,584.9	/	2022	[94]
TiO_2-CeO_2/g-C_3N_4	Thermal calcination, DFT	/	/	10 $mAcm^{-2}$	2022	[95]
porous ZnS/TiO_2	One-pot hydrothermal	Xe lamp	1,718	/	2023	[96]
20 wt% Co_9S_8/TiO_2	*In-situ* deposition hydrothermal	Xe lamp (350-780 nm)	3,982	/	2023	[97]
g-C_3N_4/TiO_2	Time-domain ab initio analysis	/	/	/	2023	[98]
TiO_2/ZnS	DFT, NAMD	/	/	/	2023	[99]
Mxene@CdS/TiO_2	/	/	16,200	9.03 μAcm^{-2}	2023	[100]
CdS/g-C_3N_4/TiO_2	Self-assemble, solvothermal, DFT	Xe lamp (200-1,000 nm)	26,840	40.2%	2023	[101]
Cu_3P/TiO_2	Microwave hydrothermal, DFT	Xe lamp	5,830	/	2023	[102]
C_3N_5/TiO_2	Sol-gel, thermally assisted *in situ* growth	Xe lamp ($\lambda > 420$ nm)	1,833.86	/	2024	[103]

Table 5. Comparison of selected research results on Other TiO_2-based heterojunction photocatalytic hydrogen evolution from 2019 to 2023

Photocatalyst	Method	Light source	H_2-production rate ($\mu molg^{-1}h^{-1}$)	IPCE/photocurrent density	Year	Ref.
MoS_2/TiO_2	DFT	/	/	/	2022	[104]
TiO_2 core-shell	*In situ* chemical growth	500 W xenon lamp	/	59.7%/3.88 $mAcm^{-2}$	2019	[105]
TiO_2@CMS/carbon-fiber	Solvothermal	Simulated-solar light	/	/	2022	[106]

self-consistency and the fact that hybridized functional calculations are unsuitable for calculating crystal structures with a large number of atoms due to their high accuracy and computational effort[109].

On the other hand, with the rapid development of DFT calculation and machine learning (ML) in the field of materials, DFT calculation can predict new heterostructures, provide new heterostructures for experiments, and allow rational design of efficient photocatalytic heterojunctions. For example, Li *et al.* used it to obtain the Gibbs free energy of RuO_2/TiO_2 as only -0.1 eV and then guided the experimental synthesis of RuO_2/TiO_2 for photocatalytic hydrogen evolution[107]. However, due to the large number of atoms (> 200) in TiO_2-based heterojunctions, the traditional DFT calculation for heterostructure prediction is highly costly and inefficient, and thus, less research has been carried out so far. Conversely, ML has the

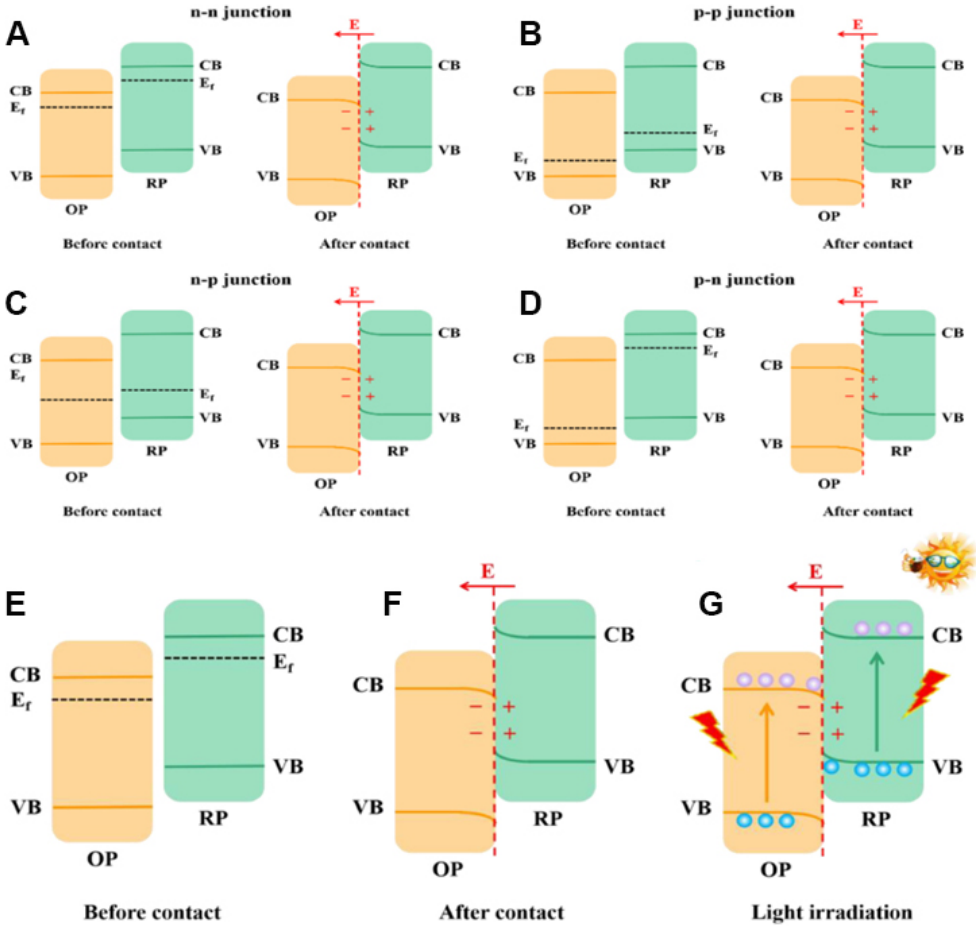

Figure 9. (A) n-n junction, (B) p-p junction, (C) n-p junction, (D) p-n junction (E-G) Photogenerated carrier migration process and photocatalytic mechanism before and after contact. Quoted with permission from Li *et al.*[87].

characteristics of high efficiency, strong model generalization ability, and self-learning ability, which solves the problem of low efficiency of DFT prediction, and can be used for high-throughput screening of heterostructures according to the set conditions[6,108]. Currently, ML is in the stage of rapid development; in future research, it can reveal the physicochemical properties of materials, quickly screen the materials that meet the conditions for the construction of heterostructures, optimize the design of catalysts, quickly find the location of active sites and factors affecting the activity of catalysts, and modulate the composition of the material, so as to guide the experiments to synthesize the higher-efficiency heterostructures.

SUMMARY AND OUTLOOK

This review systematically discusses the research progress of TiO_2-based heterojunction photocatalysts in photocatalytic hydrogen evolution since 2019. Different heterojunctions, including type-I, type-II, type-III, p-n type, Z-scheme, and the S-scheme heterojunctions, and their photocatalytic mechanisms are discussed in detail, along with their advantages and disadvantages. Direct Z- and S-scheme heterojunctions have optimal photocatalytic activity. Both generate a strong IEF at the interface to promote the separation of photogenerated carriers while maintaining a good oxidation-reduction capacity. The construction of TiO_2-based heterojunctions for photocatalytic hydrogen evolution is a promising approach to solving the energy crisis. In addition, some challenges of TiO_2-based heterojunctions still exist, outlined as follows:

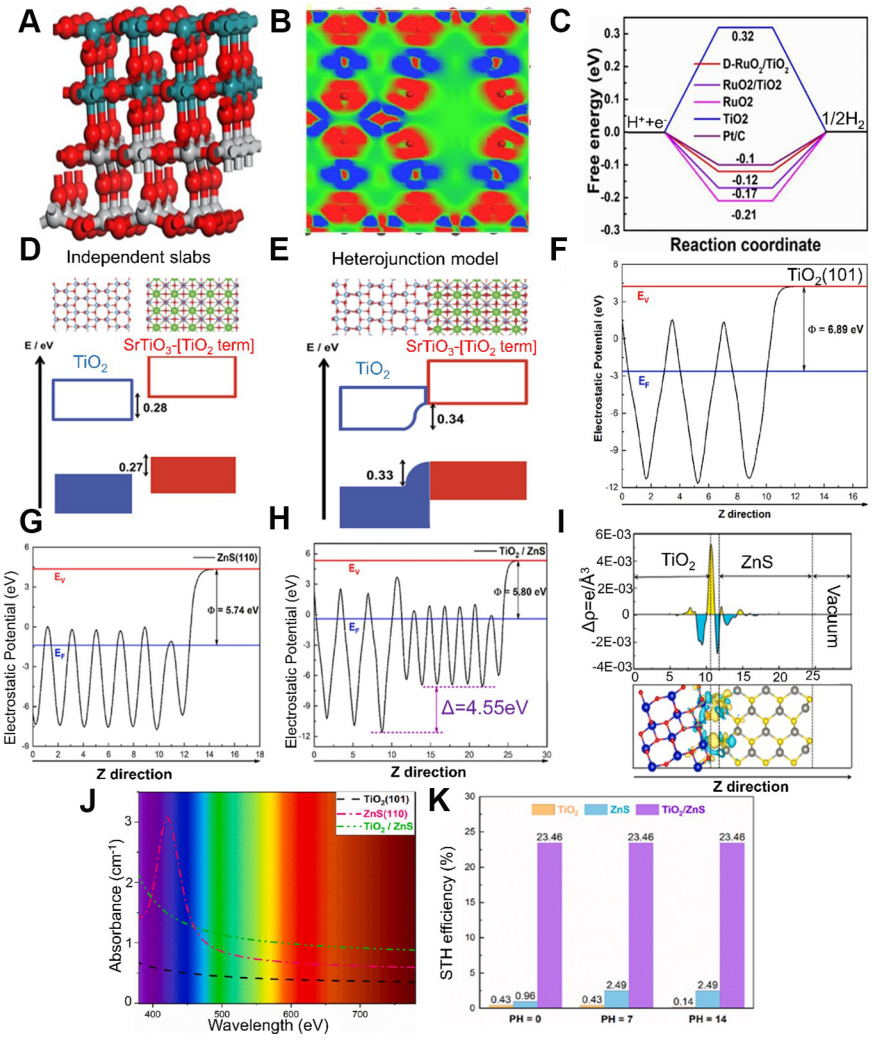

Figure 10. (A) D-RuO_2/TiO_2 nano-heterostructure, (B) Electron localization function analysis mapped, (C) ΔG_H of TiO_2, RuO_2/TiO_2, Pt/C and D-RuO_2/TiO_2. (A-C) is quoted with permission from Li *et al.*[107] Band offsets of (D) $SrTiO_3$ and TiO_2 slabs (E) $SrTiO_3$/TiO_2 heterostructure. (D and E) is quoted with permission from Di Liberto *et al.*[108] work function of (F) TiO_2(101), (G) ZnS (110), (H)TiO_2 /ZnS. (I) Planar-averaged charge density difference for the TiO_2/ZnS heterojunction. (J) Absorption spectra, (K) STH efficiency of the TiO_2 (101), ZnS (110), and TiO_2/ZnS heterojunction. (F-K) is quoted with permission from Li *et al.*[99].

(1) Among the conventional heterojunctions, type-II heterojunctions have a weak oxidation reduction capacity due to the carriers in the original catalysts that hinder the electron transfer. These problems may be overcome by modifying type-II heterojunctions into Z-type or S-type heterojunctions.

(2) The p-n heterojunctions have two types of energy band arrangements and charge transfer, in which the classification and difference between the second type of p-n junction and the Z-scheme remain greatly controversial, and more precise characterization and calculations should be employed to reveal the difference in the mechanism.

(3) The p-n heterojunction inherits most of the qualities of type-II, and the oxidation-reduction capacity of the catalyst has been improved, but it is still insufficient and hinders the development of the p-n heterojunction. Although the double p-n heterojunction can further improve the oxidation-reduction ability of the catalyst, it requires the synergistic action of three semiconductors.

(4) Direct Z-scheme heterojunction accelerates surface charge separation and reaction dynamics, but the exact mechanism of the carrier transfer in direct Z-scheme heterojunctions remains controversial currently. In addition, the bandgap of the two semiconductors in the Z scheme is easily mismatched, severely affecting the catalytic performance. In further studies, tuning the bandgap and band edge positions of the two semiconductor monomers is essential for Z-scheme heterojunctions, and the experimental characterization should be closely coupled with DFT to accurately explore the mechanism of Z-scheme heterojunctions.

(5) The S-scheme heterojunction realizes photogenerated charge separation, reduces photogenerated electrons and hole recombination through IEF and band bending, and improves the photoelectric conversion efficiency, and the generated electrons and holes have strong oxidation-reduction ability. However, it has been proposed for a short time, and its deeper action mechanism remains to be explored. Furthermore, it is unsuitable for photoelectrochemistry and is limited to powder photocatalysts. In the future, we should focus on improving the catalytic activity by adjusting the Fermi level of RP and OP and designing its surface morphology reasonably.

Developing novel and advanced photocatalysts is important to boost the photocatalytic hydrogen evolution rate. Well-constructed heterojunctions could greatly enhance the promotion of photogenerated electron-hole pair separation; thus, designing highly efficient photocatalysts with good charge separation is extremely important. To better design and synthesize high performance TiO_2-based heterojunctions, some suggestions can be considered:

(1) Current experimental characterization mostly illustrates charge transfer using XPS and photoluminescence spectroscopy, but it is not accurate to indicate whether the electron transfer is the contribution of the heterojunction or a single catalyst. Therefore, it is important to develop more advanced characterization techniques to explore the charge transfer pathway, such as high spatial and temporal *in situ* detection at the atomic level, high precision time-resolved surface photovoltage (SPV) imaging and scanning tunneling microscopy.

(2) Employing more accurate DFT computation methods, such as time-containing DFT, transient DFT, and transient charge-carrier dynamics, can provide more precise evidence for the charge-transfer paths and migration dynamics of heterojunctions.

(3) The rapid development of ML provides more accurate predictions for the experimental synthesis of semiconductor heterojunctions. Conventional DFT is inefficient and time-consuming because it can only couple heterojunctions one by one and then simulate and predict their catalyst performance. However, ML is an efficient and economical approach to synthesizing thousands of heterojunctions and obtaining semiconductor heterojunctions with excellent catalyst performance through the high-throughput screening. In a word, the advancement of ML will further promote the development of photocatalysts.

DECLARATIONS

Authors' contributions

Literature search and organization and manuscript drafting: Yang N, He T
Manuscript revision: Zhang G, Chen X, He Y, Zhou T
Project supervision: He T, Liu Q

Availability of data and materials
Not applicable.

Financial support and sponsorship
This work received funding from the National Key Research and Development Program of China (2022YFB3803600), the National Natural Science Foundation of China (22378346, 22368050), and the Key Research and Development Program of Yunnan Province (202302AF080002).

Conflicts of interest
All authors declared that there are no conflicts of interest.

Ethical approval and consent to participate
Not applicable.

Consent for publication
Not applicable.

REFERENCES
1. Chen M, Rao P, Miao Z, et al. Strong metal-support interaction of Pt-based electrocatalysts with transition metal oxides/nitrides/carbides for oxygen reduction reaction. *Microstructures* 2023;3:2023025. DOI
2. Liu N, Liu Y, Liu Y, Li Y, Cheng Y, Li H. Modulation of photogenerated holes for enhanced photoelectrocatalytic performance. *Microstructures* 2022;3:2023001. DOI
3. Zhou A, Wang D, Li Y. Hollow microstructural regulation of single-atom catalysts for optimized electrocatalytic performance. *Microstructures* 2022;2:2022005. DOI
4. He T, Puente-santiago AR, Xia S, Ahsan MA, Xu G, Luque R. Experimental and theoretical advances on single atom and atomic cluster-decorated low-dimensional platforms towards superior electrocatalysts. *Adv Energy Mater* 2022;12:2200493. DOI
5. Zhao X, Li J, Kong X, et al. Carbon dots mediated in situ confined growth of Bi clusters on g-C_3N_4 nanomeshes for boosting plasma-assisted photoreduction of CO_2. *Small* 2022;18:e2204154. DOI
6. Ahsan MA, He T, Noveron JC, Reuter K, Puente-Santiago AR, Luque R. Low-dimensional heterostructures for advanced electrocatalysis: an experimental and computational perspective. *Chem Soc Rev* 2022;51:812-28. DOI PubMed
7. Kong Y, Li X, Puente Santiago AR, He T. Nonmetal atom doping induced orbital shifts and charge modulation at the edge of two-dimensional boron carbonitride leading to enhanced photocatalytic nitrogen reduction. *J Am Chem Soc* 2024;146:5987-97. DOI
8. He T, Exner KS. Computational electrochemistry focusing on nanostructured catalysts: challenges and opportunities. *Mater Today Energy* 2022;28:101083. DOI
9. Fujishima A, Honda K. Electrochemical photolysis of water at a semiconductor electrode. *Nature* 1972;238:37-8. DOI
10. Guo Q, Zhou C, Ma Z, Yang X. Fundamentals of TiO_2 photocatalysis: concepts, mechanisms, and challenges. *Adv Mater* 2019;31:e1901997. DOI PubMed
11. Dakhel AA. Hydrogenation influences on the structural, optical, and insulating properties of (Bi+Cr) codoped anatase TiO_2 nanoparticles. *Cryst Res Technol* 2023;58:2300016. DOI
12. Nolan M, Iwaszuk A, Lucid AK, Carey JJ, Fronzi M. Design of novel visible light active photocatalyst materials: surface modified TiO_2. *Adv Mater* 2016;28:5425-46. DOI PubMed
13. Guo P, Fu X, Deák P, Frauenheim T, Xiao J. Activity and mechanism mapping of photocatalytic NO_2 conversion on the anatase TiO_2(101) surface. *J Phys Chem Lett* 2021;12:7708-16. DOI
14. Alcudia-ramos M, Fuentez-torres M, Ortiz-chi F, et al. Fabrication of g-C_3N_4/TiO_2 heterojunction composite for enhanced photocatalytic hydrogen production. *Ceram Int* 2020;46:38-45. DOI
15. Zhou L, Zhang X, Cai M, Cui N, Chen G, Zou G. New insights into the efficient charge transfer of the modified-TiO_2/Ag_3PO_4 composite for enhanced photocatalytic destruction of algal cells under visible light. *Appl Catal B Environ* 2022;302:120868. DOI
16. Xia B, He B, Zhang J, et al. TiO_2 /$FePS_3$ S-scheme heterojunction for greatly raised photocatalytic hydrogen evolution. *Adv Energy Mater* 2022;12:2201449. DOI
17. Wei L, Yu C, Zhang Q, Liu H, Wang Y. TiO_2-based heterojunction photocatalysts for photocatalytic reduction of CO_2 into solar fuels. *J Mater Chem A* 2018;6:22411-36. DOI
18. Xu F, Zhang J, Zhu B, Yu J, Xu J. $CuInS_2$ sensitized TiO_2 hybrid nanofibers for improved photocatalytic CO_2 reduction. *Appl Catal B*

Environ 2018;230:194-202. DOI

19. Eidsvåg H, Bentouba S, Vajeeston P, Yohi S, Velauthapillai D. TiO_2 as a photocatalyst for water splitting-an experimental and theoretical review. *Molecules* 2021;26:1687. DOI PubMed PMC
20. Li K, Teng C, Wang S, Min Q. Recent advances in TiO_2-based heterojunctions for photocatalytic CO_2 reduction with water oxidation: a review. *Front Chem* 2021;9:637501. DOI PubMed PMC
21. Ijaz M, Zafar M. Titanium dioxide nanostructures as efficient photocatalyst: progress, challenges and perspective. *Int J Energy Res* 2021;45:3569-89. DOI
22. Gao J, Xue J, Shen Q, et al. A promoted photocatalysis system trade-off between thermodynamic and kinetic via hierarchical distribution dual-defects for efficient H_2 evolution. *Chem Eng J* 2022;431:133281. DOI
23. An X, Wei T, Ding P, et al. Sodium-directed photon-induced assembly strategy for preparing multisite catalysts with high atomic utilization efficiency. *J Am Chem Soc* 2023;145:1759-68. DOI
24. Wang W, Li G, An T, Chan DK, Yu JC, Wong PK. Photocatalytic hydrogen evolution and bacterial inactivation utilizing sonochemical-synthesized g-C_3N_4/red phosphorus hybrid nanosheets as a wide-spectral-responsive photocatalyst: the role of type I band alignment. *Appl Catal B Environ* 2018;238:126-35. DOI
25. Huang Z, Zhao S, Yu Y. Experimental method to explore the adaptation degree of type-II and all-solid-state Z-scheme heterojunction structures in the same degradation system. *Chinese J Catal* 2020;41:1522-34. DOI
26. Hyun JK, Zhang S, Lauhon LJ. Nanowire heterostructures. *Annu Rev Mater Res* 2013;43:451-79. DOI
27. Kuang X, Deng X, Ma Y, et al. Type II heterojunction promotes photoinduced effects of TiO_2 for enhancing photocatalytic performance. *J Mater Chem C* 2022;10:6341-7. DOI
28. Xia C, Guo RT, Bi ZX, Zhang ZR, Li CF, Pan WG. A dual Z-scheme heterojunction Cu-CuTCPP/Cu_2O/CoAl-LDH for photocatalytic CO_2 reduction to C_1 and C_2 products. *Dalton Trans* 2023;52:12742-54. DOI PubMed
29. Xu Q, Zhang L, Cheng B, Fan J, Yu J. S-Scheme heterojunction photocatalyst. *Chem* 2020;6:1543-59. DOI
30. Low J, Yu J, Jaroniec M, Wageh S, Al-Ghamdi AA. Heterojunction photocatalysts. *Adv Mater* 2017;29:1601694. DOI PubMed
31. Zhao Y, Linghu X, Shu Y, et al. Classification and catalytic mechanisms of heterojunction photocatalysts and the application of titanium dioxide (TiO_2)-based heterojunctions in environmental remediation. *J Environ Chem Eng* 2022;10:108077. DOI
32. Shi W, Chopra N. Nanoscale heterostructures for photoelectrochemical water splitting and photodegradation of pollutants. *Nanomater Energy* 2013;2:158-78. DOI
33. Cao J, Zhang J, Guo W, et al. A type-I heterojunction by anchoring ultrafine Cu_2O on defective TiO_2 framework for efficient photocatalytic H_2 production. *Ind Eng Chem Res* 2023;62:1310-21. DOI
34. Luo X, Ke Y, Yu L, et al. Tandem CdS/TiO_2(B) nanosheet photocatalysts for enhanced H_2 evolution. *Appl Surf Sci* 2020;515:145970. DOI
35. Park J, Lee TH, Kim C, et al. Hydrothermally obtained type-II heterojunction nanostructures of In_2S_3/TiO_2 for remarkably enhanced photoelectrochemical water splitting. *Appl Catal B Environ* 2021;295:120276. DOI
36. Zhou BX, Ding SS, Wang Y, et al. Type-II/type-II band alignment to boost spatial charge separation: a case study of g-C_3N_4 quantum dots/a-TiO_2/r-TiO_2 for highly efficient photocatalytic hydrogen and oxygen evolution. *Nanoscale* 2020;12:6037-46. DOI
37. Yang W, Hou H, Yang Y, et al. MXene-derived anatase-TiO_2/rutile-TiO_2/In_2O_3 heterojunctions toward efficient hydrogen evolution. *Colloids Surf A* 2022;652:129881. DOI
38. Li H, Chen ZH, Zhao L, Yang GD. Synthesis of TiO_2@$ZnIn_2S_4$ hollow nanospheres with enhanced photocatalytic hydrogen evolution. *Rare Met* 2019;38:420-7. DOI
39. Zhang L, Huang Y, Dai C, et al. Constructing ZnO/$ZnCr_2O_4$@TiO_2-NTA nanocomposite for photovoltaic conversion and photocatalytic hydrogen evolution. *J Electron Mater* 2019;48:1724-9. DOI
40. Huang K, Li C, Meng X. In-situ construction of ternary Ti_3C_2 MXene@TiO_2/$ZnIn_2S_4$ composites for highly efficient photocatalytic hydrogen evolution. *J Colloid Interface Sci* 2020;580:669-80. DOI
41. Sadeghzadeh-Attar A. Boosting the photocatalytic ability of hybrid $BiVO_4$-TiO_2 heterostructure nanocomposites for H_2 production by reduced graphene oxide (rGO). *J Taiwan Inst Chem Eng* 2020;111:325-36. DOI
42. Qin Y, Li H, Lu J, et al. Nitrogen-doped hydrogenated TiO_2 modified with CdS nanorods with enhanced optical absorption, charge separation and photocatalytic hydrogen evolution. *Chem Eng J* 2020;384:123275. DOI
43. Niu M, Sui K, Wu X, Cao D, Liu C. GaAs quantum dot/TiO_2 heterojunction for visible-light photocatalytic hydrogen evolution: promotion of oxygen vacancy. *Adv Compos Hybrid Mater* 2022;5:450-60. DOI
44. Peng H, Yong J, Wang H, Gou Y, Wang F, Zheng X. Dual CdS-CoS/S,N-doped TiO_2 nanofibers for efficient visible-light induced H_2 evolution. *Int J Hydrogen Energy* 2022;47:31269-78. DOI
45. Liu D, Liang H, Li C, Bai J. CdS nanoparticles with highly exposed (111) facets decorated on Pt/TiO_2 nanotubes for highly efficient photocatalytic H_2 evolution. *Appl Surf Sci* 2022;586:152711. DOI
46. Lin Y, Fang W, Xv R, Fu L. TiO_2 nanoparticles modified with $ZnIn_2S_4$ nanosheets and Co-Pi groups: type II heterojunction and cocatalysts coexisted photoanode for efficient photoelectrochemical water splitting. *Int J Hydrogen Energy* 2022;47:33361-73. DOI
47. Huo Y, Tian Y, Hu T, et al. CdS-loaded three-dimensional ordered macroporous composite material In_2O_3-TiO_2: construction of type II heterostructure and enhancement of photocatalytic performance. *Appl Catal A Gen* 2023;652:119042. DOI
48. Yavuz C, Ela SE. Fabrication of g g-C_3N_4-reinforced CdS nanosphere-decorated TiO_2 nanotablet composite material for photocatalytic hydrogen production and dye-sensitized solar cell application. *J Alloys Compd* 2023;936:168209. DOI

49. Ding Y, Zhang J, Yang Y, et al. Fully-depleted dual P-N heterojunction with type-II band alignment and matched build-in electric field for high-efficient photocatalytic hydrogen production. *Int J Hydrogen Energy* 2021;46:36069-79. DOI
50. Liu J, Sun X, Fan Y, et al. P-N heterojunction embedded CuS/TiO_2 bifunctional photocatalyst for synchronous hydrogen production and benzylamine conversion. *Small* 2024;20:e2306344. DOI
51. Wang Y, Zhu C, Zuo G, et al. 0D/2D Co_3O_4/TiO_2 Z-scheme heterojunction for boosted photocatalytic degradation and mechanism investigation. *Appl Catal B Environ* 2020;278:119298. DOI
52. Wang Z, Lin Z, Shen S, Zhong W, Cao S. Advances in designing heterojunction photocatalytic materials. *Chin J Catal* 2021;42:710-30. DOI
53. Xing C, Liu Y, Zhang Y, et al. A direct Z-scheme for the photocatalytic hydrogen production from a water ethanol mixture on $CoTiO_3$/TiO_2 heterostructures. *ACS Appl Mater Interfaces* 2021;13:449-57. DOI
54. Wang L, Tang G, Liu S, et al. Interfacial active-site-rich 0D Co_3O_4/1D TiO_2 p-n heterojunction for enhanced photocatalytic hydrogen evolution. *Chem Eng J* 2022;428:131338. DOI
55. Chen B, Yu J, Wang R, et al. Three-dimensional ordered macroporous g-C_3N_4-Cu_2O-TiO_2 heterojunction for enhanced hydrogen production. *Sci China Mater* 2022;65:139-46. DOI
56. Qiu D, He C, Lu Y, Li Q, Chen Y, Cui X. Assembling γ-graphyne surrounding TiO_2 nanotube arrays: an efficient p-n heterojunction for boosting photoelectrochemical water splitting. *Dalton Trans* 2021;50:15422-32. DOI
57. Zheng D, Zhao H, Wang S, Hu J, Chen Z. NiO-TiO_2 p-n heterojunction for solar hydrogen generation. *Catalysts* 2021;11:1427. DOI
58. Feng K, Sun T, Hu X, Fan J, Yang D, Liu E. 0D/2D Co0.85Se/TiO_2 p-n heterojunction for enhanced photocatalytic H_2 evolution. *Catal Sci Technol* 2022;12:4893-902. DOI
59. Huang W, Fu Z, Hu X, Wang Q, Fan J, Liu E. Efficient photocatalytic hydrogen evolution over $Cu_3Mo_2O_9$/TiO_2 p-n heterojunction. *J Alloys Compd* 2022;904:164089. DOI
60. Pan J, Xiao G, Niu J, et al. The photocatalytic hydrogen evolution and photoreduction CO_2 selective enhancement of Co_3O_4/Ti^{3+}-TiO_2 /NiO hollow core-shell dual pn junction. *J Clean Prod* 2022;380:135037. DOI
61. Dhileepan MD, Lakhera SK, Neppolian B. Interface engineering of 0D-1D Cu_2NiSnS_4/TiO_2(B) p-n heterojunction nanowires for efficient photocatalytic hydrogen evolution. *Catal Today* 2023;423:114006. DOI
62. Yuan X, Tang S, Liu X. A Li-F co-doped g-C_3N_4/TiO_2-B (001) heterostructure as an efficient hydrogen evolution photocatalyst. *Sustain Energy Fuels* 2023;7:1633-44. DOI
63. Wang C, Xiong J, Wen Z, Cheng G. Integrated $Ni(OH)_2$-TiO_2-Cu_2O hybrids with a synergic impact of the p-n heterojunction/cocatalyst for enhanced photocatalytic hydrogen production. *Ind Eng Chem Res* 2023;62:11402-13. DOI
64. Eisapour M, Zhao H, Zhao J, et al. p-n heterojunction of nickel oxide on titanium dioxide nanosheets for hydrogen and value-added chemicals coproduction from glycerol photoreforming. *J Colloid Interface Sci* 2023;647:255-63. DOI
65. Bai S, Jiang J, Zhang Q, Xiong Y. Steering charge kinetics in photocatalysis: intersection of materials syntheses, characterization techniques and theoretical simulations. *Chem Soc Rev* 2015;44:2893-939. DOI PubMed
66. Han X, Dong Y, Zhao J, Ming S, Xie Y. Construction of ternary Z-scheme covalent triazine framework@Au@TiO_2 for enhanced visible-light-driven hydrogen evolution activity. *Int J Hydrogen Energy* 2022;47:18334-46. DOI
67. Wang X, Liu G, Chen ZG, et al. Enhanced photocatalytic hydrogen evolution by prolonging the lifetime of carriers in ZnO/CdS heterostructures. *Chem Commun* 2009;23:3452-4. DOI
68. Yu J, Wang S, Low J, Xiao W. Enhanced photocatalytic performance of direct Z-scheme g-C_3N_4-TiO_2 photocatalysts for the decomposition of formaldehyde in air. *Phys Chem Chem Phys* 2013;15:16883-90. DOI
69. Ran J, Chen L, Wang D, et al. Atomic-level regulated 2D $ReSe_2$: a universal platform boostin photocatalysis. *Adv Mater* 2023;35:2210164. DOI
70. Moon HS, Hsiao KC, Wu MC, Yun Y, Hsu YJ, Yong K. Spatial separation of cocatalysts on z-scheme organic/inorganic heterostructure hollow spheres for enhanced photocatalytic H_2 evolution and in-depth analysis of the charge-transfer mechanism. *Adv Mater* 2023;35:e2200172. DOI PubMed
71. Zuo G, Wang Y, Teo WL, Xian Q, Zhao Y. Direct Z-scheme TiO_2-$ZnIn_2S_4$ nanoflowers for cocatalyst-free photocatalytic water splitting. *Appl Catal B Environ* 2021;291:120126. DOI
72. Sun F, Xie Y, Xu D, et al. Electrospun self-supporting double Z-scheme tricolor-typed microfiber oriented-heterostructure photocatalyst with highly effective hydrogen evolution and organic pollutants degradation. *J Environ Chem Eng* 2023;11:109169. DOI
73. Wang J, Wang G, Wang X, Wu Y, Su Y, Tang H. 3D/2D direct Z-scheme heterojunctions of hierarchical TiO_2 microflowers/g-C_3N_4 nanosheets with enhanced charge carrier separation for photocatalytic H_2 evolution. *Carbon* 2019;149:618-26. DOI
74. Ke X, Zhang J, Dai K, Liang C. Construction of flourinated-TiO_2 nanosheets with exposed {001} facets/CdSe-DETA nanojunction for enhancing visible-light-driven photocatalytic H_2 evolution. *Ceram Int* 2020;46:866-76. DOI
75. Zhang M, Piao C, Wang D, et al. Fixed Z-scheme TiO_2|Ti|WO_3 composite film as recyclable and reusable photocatalyst for highly effective hydrogen production. *Opt Mater* 2020;99:109545. DOI
76. Drmosh Q, Hezam A, Hendi A, Qamar M, Yamani Z, Byrappa K. Ternary Bi_2S_3/MoS_2/TiO_2 with double Z-scheme configuration as high performance photocatalyst. *Appl Surf Sci* 2020;499:143938. DOI
77. Subha N, Mahalakshmi M, Monika S, Neppolian B. $Ni(OH)_2$-Cu_xO-TiO_2 nanocomposite for the enhanced H_2 production under solar light: the mechanistic pathway. *Int J Hydrogen Energy* 2020;45:7552-61. DOI

78. Du Y, Wang N, Li X, et al. A facile synthesis of C_3N_4-modified TiO_2 nanotube embedded Pt nanoparticles for photocatalytic water splitting. *Res Chem Intermed* 2021;47:5175-88. DOI
79. Zhang Y, Liu M, Chen J, Xie K, Fang S. Dendritic branching Z-scheme Cu_2O/TiO_2 heterostructure photocatalysts for boosting H_2 production. *J Phys Chem Solids* 2021;152:109948. DOI
80. Priya B, Sivakumar T, Venkateswari P. Construction of MoS_2 nanoparticles incorporated TiO_2 nanosheets heterojunction photocatalyst for enhanced visible light driven hydrogen production. *Inorg Chem Comm* 2022;136:109118. DOI
81. Du R, Li B, Han X, et al. 2D/2D Heterojunction of TiO_2 nanoparticles and ultrathin G-C_3N_4 nanosheets for efficient photocatalytic hydrogen evolution. *Nanomaterials* 2022;12:1557. DOI PubMed PMC
82. He Y, Zheng H, Lv T, et al. MOFs-derived TiO_2 composite $ZnIn_2S_4$ to construct Z-scheme heterojunction for efficient photocatalytic hydrogen evolution under visible light. *J Environ Chem Eng* 2023;11:111224. DOI
83. Wang YQ, Yang C, Gan LH. Preparation of direct Z-scheme Bi_2WO_6/TiO_2 heterojunction by one-step solvothermal method and enhancement mechanism of photocatalytic H_2 production. *Int J Hydrogen Energy* 2023;48:19372-84. DOI
84. Zhao SZ, Lu R, Yang Y, Lu Y, Rodriguez RD, Chen JJ. Direct Z-scheme g-C_3N_4/TiO_2 heterojunction porous nanotubes: an ingenious synthesis strategy to enhance photocatalytic activity. *J Environ Chem Eng* 2023;11:109366. DOI
85. Zhu Y, Ren J, Huang G, et al. Red phosphorus grafted high-index (116) faceted anatase TiO_2 for Z-scheme photocatalytic pure water splitting. *Adv Funct Mater* 2024;34:2311623. DOI
86. Zhang L, Zhang J, Yu H, Yu J. Emerging S-scheme photocatalyst. *Adv Mater* 2022;34:e2107668. DOI
87. Li T, Tsubaki N, Jin Z. S-scheme heterojunction in photocatalytic hydrogen production. *J Mater Sci Technol* 2024;169:82-104. DOI
88. Bootluck W, Chittrakarn T, Techato K, Jutaporn P, Khongnakorn W. S-Scheme α-Fe_2O_3/TiO_2 photocatalyst with Pd cocatalyst for enhanced photocatalytic H_2 production activity and stability. *Catal Lett* 2022;152:2590-606. DOI
89. Dong G, Zhang Y, Wang Y, et al. Ti_3C_2 quantum dots modified 3D/2D TiO_2/g-C_3N_4 S-scheme heterostructures for highly efficient photocatalytic hydrogen evolution. *ACS Appl Energy Mater* 2021;4:14342-51. DOI
90. Chen L, Song XL, Ren JT, Yuan ZY. Precisely modifying Co_2P/black TiO_2 S-scheme heterojunction by *in situ* formed P and C dopants for enhanced photocatalytic H_2 production. *Appl Catal B Environ* 2022;315:121546. DOI
91. Dai X, Feng S, Wu W, et al. Photocatalytic hydrogen evolution and antibiotic degradation by S-scheme $ZnCo_2S_4/TiO_2$. *Int J Hydrogen Energy* 2022;47:25104-16. DOI
92. Huang W, Xue W, Hu X, Fan J, Tang C, Liu E. Photocatalytic H_2 production over S-scheme Co_3Se_4/TiO_2 nanosheet with super-hydrophilic surface. *Appl Surf Sci* 2022;599:153900. DOI
93. Li J, Wu C, Li J, Dong B, Zhao L, Wang S. 1D/2D $TiO_2/ZnIn_2S_4$ S-scheme heterojunction photocatalyst for efficient hydrogen evolution. *Chin J Catal* 2022;43:339-49. DOI
94. Liu J, Wan J, Liu L, et al. Synergistic effect of oxygen defect and doping engineering on S-scheme O-$ZnIn_2S_4/TiO_{2-x}$ heterojunction for effective photocatalytic hydrogen production by water reduction coupled with oxidative dehydrogenation. *Chem Eng J* 2022;430:133125. DOI
95. Vignesh S, Chandrasekaran S, Srinivasan M, et al. T TiO_2-CeO_2/g-C_3N_4 S-scheme heterostructure composite for enhanced photo-degradation and hydrogen evolution performance with combined experimental and DFT study. *Chemosphere* 2022;288:132611. DOI
96. Gui X, Zhou Y, Liang Q, et al. Construction of porous ZnS/TiO_2 S-scheme heterostructure derived from MOF-on-MOF with boosting photocatalytic H_2-generation activity. *Int J Hydrogen Energy* 2023;48:38237-50. DOI
97. Huang W, Xue W, Hu X, et al. A S-scheme heterojunction of Co_9S_8 decorated TiO_2 for enhanced photocatalytic H_2 evolution. *J Alloys Compd* 2023;930:167368. DOI
98. Wu X, Chen G, Wang J, Li J, Wang G. Review on S-scheme heterojunctions for photocatalytic hydrogen evolution. *Acta Phys Chim Sin* 2023;39:2212016. DOI
99. Li D, Li R, Zhou D, Qin X, Yan W. S-scheme TiO_2/ZnS heterojunction as dual-reaction sites: a high-efficiency and spontaneous photocatalyst for hydrogen production under light irradiation. *Vacuum* 2023;210:111906. DOI
100. Navakoteswara Rao V, Kwon H, Lee Y, et al. Synergistic integration of MXene nanosheets with CdS@TiO_2 core@shell S-scheme photocatalyst for augmented hydrogen generation. *Chem Eng J* 2023;471:144490. DOI
101. Ruan X, Meng D, Huang C, et al. Artificial photosynthetic system with spatial dual reduction site enabling enhanced solar hydrogen production. *Adv Mater* 2024;36:e2309199. DOI
102. Wang K, Luo Z, Xiao B, et al. S-scheme Cu_3P/TiO_2 heterojunction for outstanding photocatalytic water splitting. *J Colloid Interface Sci* 2023;652:1908-16. DOI
103. Chen S, Sheng X, Wang Y, et al. Thermally assisted in situ synthesis of C_3N_5/TiO_2 S-scheme heterojunctions with enhanced visible light response for photocatalytic hydrogen precipitation. *Appl Surf Sci* 2024;643:158600. DOI
104. Tang Y, Liu Q, Lei J, et al. MoS_2/TiO_2 van der Waals heterostructures for promising photocatalytic performance: a first-principles study. *Mater Res Express* 2022;9:105502. DOI
105. Wei N, Liu Y, Feng M, et al. Controllable TiO_2 core-shell phase heterojunction for efficient photoelectrochemical water splitting under solar light. *Appl Catal B Environ* 2019;244:519-28. DOI
106. Chen HJ, Yang YL, Zou XX, Shi XL, Chen ZG. Flexible hollow TiO_2@CMS/carbon-fiber van der Waals heterostructures for simulated-solar light photocatalysis and photoelectrocatalysis. *J Mater Sci Technol* 2022;98:143-50. DOI
107. Li W, Zhang H, Hong M, et al. Defective RuO_2/TiO_2 nano-heterostructure advances hydrogen production by electrochemical water splitting. *Chem Eng J* 2022;431:134072. DOI

108. Di Liberto G, Tosoni S, Illas F, et al. Nature of $SrTiO_3/TiO_2$ (anatase) heterostructure from hybrid density functional theory calculations. *J Chem Phys* 2020;152:184704. DOI

109. Chen W, Yuan P, Zhang S, Sun Q, Liang E, Jia Y. Electronic properties of anatase TiO_2 doped by lanthanides: A DFT+U study. *Phys B Condens Matter* 2012;407:1038-43. DOI